https://doi.org/10.5194/egusphere-2026-3397
Preprint. Discussion started: 29 July 2026

Diurnal and seasonal variability of ozone-precursor relationships in a semi-arid urban environment

Megan L. Robertson[1], Chayan Roychoudhury[1], Keming Pan[1], Mohammad Amin Mirrezaei[1], Armin Sorooshian[2], and Avelino F. Arellano[1]

[1]Hydrology and Atmospheric Sciences, University of Arizona, Tucson, 85721, United States
[2]Chemical and Environmental Engineering, University of Arizona, Tucson, 85721, United States

Correspondence to: Megan L. Robertson (megrobertson@arizona.edu)

Abstract. The southwestern United States is characterized by arid meteorology, responsive vegetation, intense solar radiation, anthropogenic emissions, and dust events that shape regional air quality. Elevated ground-level ozone (O_3) concentrations are a primary air quality concern, driven by interactions between chemical precursors, including nitrogen oxides (NO_x) and volatile organic compounds (VOCs), and meteorological variables. We examine these dynamics over Tucson, Arizona, using a multi-platform correlation analysis of satellite total-column measurements from Tropospheric Emissions: Monitoring of Pollution (TEMPO), ground-based total-column and surface measurements from Pandora, surface measurements from U.S. EPA Air Quality System (AQS), and lidar-derived planetary boundary layer height (PBLH). We address three objectives: (1) characterize the diurnal and seasonal evolution of tropospheric nitrogen dioxide (NO_2) and formaldehyde (HCHO), (2) quantify the strength and variability of O_3-precursor relationships across diurnal and seasonal timescales, and (3) investigate evidence of nonlinear O_3 formation behavior. We show that tropospheric O_3 precursors exhibit distinct diurnal and seasonal trends with NO_2 peaking during winter nighttime, HCHO peaking during monsoon summer with concentrations 2.5-3.7 times higher than non-monsoon periods, and O_3 peaking in late spring and summer afternoons. The strongest O_3-NO_2 and O_3-HCHO correlations occur during summer afternoons and when HCHO precedes O_3 by several hours, respectively. Evidence of nonlinear O_3 behavior emerges through seasonal shifts in diurnal correlation structure. PBLH-normalization improves column-surface agreement for NO_2 but not HCHO. These results highlight the importance of meteorology-chemistry-emissions coupling and the need to implement various observational contexts when interpreting precursor observations for O_3 mitigation.

1 Introduction

Tropospheric Ozone (O_3) is a secondary pollutant, formed through sunlight-initiated reactions of its precursors, volatile organic compounds (VOCs) and nitrogen oxides (NO_x = nitrogen dioxide (NO_2) + nitric oxide (NO)), rather than through direct emissions (Finlayson-Pitts and Pitts, 1993). Thus, O_3 concentrations are inherently linked to the emissions of its precursors, meteorology, and competing chemical reactions that determine rates of production and loss (Monks et al., 2015). When these complex factors align, elevated concentrations of O_3 pose substantial risks to both human health and ecosystems. O_3 is a respiratory irritant linked to chronic illnesses such as asthma and chronic obstructive pulmonary disease (COPD).

https://doi.org/10.5194/egusphere-2026-3397
Preprint. Discussion started: 29 July 2026

Epidemiological studies have shown that an increase of 10 ppb in O_3 concentrations results in a 1.1% increase in the hazard of all-cause mortality (Di et al., 2017). In addition to the health impacts posed by O_3, it is also phytotoxic, reducing crop yield and damaging ecological health and environmental sustainability (Ramya et al., 2023). Thus, having a comprehensive understanding of the processes controlling the variability of O_3 is imperative for the protection of human health and environmental management.

These impacts are especially visible in semi-arid to arid regions such as the desert southwestern United States, where favorable environmental conditions often result in the rapid accumulation of O_3. In Arizona, the intense sunlight and high temperatures enhance photochemical reaction rates, and precipitation events stimulate soil and vegetation, enhancing biogenic emissions and amplifying the potential for O_3 build up (Sorooshian et al., 2024). This already favorable environment for O_3 production is further complicated by the North American Monsoon, which contributes to variability of O_3 concentrations by introducing sudden variations in moisture, cloud cover, and mixing (Malloy, 2018; Malloy and Cerveny, 2019). In addition, these regions are particularly responsive to climate change, such that increasing temperatures can increase O_3 production even in the absence of changes in precursor emissions, also known as the climate penalty (Fu and Tian, 2019; Fiore et al., 2015; Parakkat et al., 2025). Thus, O_3 behavior in Arizona's Sun Corridor (a region of exceptional solar intensity and rapid urban growth connecting Phoenix and Tucson) is highly variable and necessitates a multi-platform investigation of the impacts of chemistry and meteorology on O_3 formation. Despite its unique O_3 environment, Tucson, which is the southern anchor of the Sun Corridor, has received disproportionately less scientific attention relative to Phoenix (Ajayi et al., 2025), representing a critical gap with implications for O_3 research in semi-arid and arid urban regions globally (Mirrezaei et al., 2024).

Fundamentally, O_3 formation is determined by nonlinear chemical interactions of VOCs, NO_x, and the cycling of radicals (Sillman, 2002; Monks, 2015; Pusede and Cohen, 2012). Specifically, O_3 is produced when the oxidation of VOCs produces peroxy radicals which recycle NO into NO_2, resulting in a net production of O_3, whereas competing processes such as NO titration limit O_3 accumulation (Finlayson-Pitts and Pitts, 1993; Monks et al., 2015). The efficiency of these competing processes is dependent upon the relative abundance of both VOCs and NO_x, resulting in either VOC or NO_x-limited chemical regimes (Sillman, 2002; Kleinman, 2005). These regimes vary temporally across diurnal and seasonal timescales, reflecting changes in emissions, radiation, and mixing as a function of time of day and season, which in turn drive a temporal dependence of O_3 to its precursors (Jin et al., 2020). Meteorological shifts across diurnal and seasonal timescales also modify these relationships, such that the variability of O_3 is dependent upon both chemistry and meteorology, rather than through a single factor (Fiore et al., 2012; Fiore et al., 2015; von Schneidemesser et al., 2015). O_3 concentrations vary with nonlinear and time-dependent chemical and meteorological relationships; hence, correlations between O_3 and its precursors should be interpreted within the context of these coupled chemical and meteorological processes.

https://doi.org/10.5194/egusphere-2026-3397
Preprint. Discussion started: 29 July 2026

However, effectively diagnosing these O_3-precursor relationships from an observational standpoint requires leveraging multiple observational platforms that together provide complementary temporal, spatial, and chemical species information. In particular, key O_3 precursors such as formaldehyde (HCHO), which stems from both anthropogenic and biogenic sources and carries information on VOC reactivity, are routinely under-sampled or absent from surface monitoring networks both in the United States and globally (Zhu et al., 2017; Wang et al., 2022; De Smedt et al., 2015). Surface observations, while directly relevant to human and agricultural exposure, are spatially limited and do not capture the vertical structure of precursors that influence tropospheric O_3 formation (Fishman et al. 2008). Conversely, satellite column measurements capture broad spatial distributions of O_3 precursors across local to regional scales, but their almost null vertical sensitivity limits the ability to resolve planetary boundary layer (PBL) processes, particularly for short-lived species such as HCHO and NO_2, whose surface concentrations and column abundances can differ substantially depending on planetary boundary layer height (PBLH), mixing, and local emission sources (Fishman et al. 2008; Wang et al., 2022). Ground-based remote sensing instruments, including Pandora spectrometers and lidar, offer complementary strengths, such that Pandora provides high-precision total and tropospheric columns of NO_2 and HCHO (Herman et al., 2009; Rawat et al., 2025), and lidar-derived PBLHs constrain vertical mixing and improve the translation of column observations to surface concentrations (Lamsal et al., 2008; Knepp et al. 2015; Sullivan et al., 2019). Geostationary and low-earth orbit satellite platforms, such as TEMPO (Zoogman et al. 2017), TROPOMI (Veefkind et al. 2012), and OMI (Levelt et al., 2018), provide high temporal and spatial resolution observations of atmospheric composition, yet their utility for diagnosing regional O_3-precursor relationships depends on ground-based validation and interpretation (Verhoelst et al., 2021; Rawat et al., 2025). Establishing relationships between ground-level O_3 and Pandora-derived columns of HCHO and NO_2 provides this observational bridge. Thus, the use of surface, ground-based remote sensing, and satellite observations enables a robust diagnosis of O_3-precursor relationships and their chemical and meteorological drivers, with insights transferrable to semi-arid urban environments globally.

Here, we use these observations to characterize O_3 formation and its chemical and meteorological drivers in a specific site within Arizona's Sun Corridor with three specific objectives: (1) examine the diurnal and seasonal evolution of NO_2, HCHO, and O_3 over Tucson, Arizona in 2024 to 2025 using Pandora column observations, U.S. EPA AQS surface measurements, and ground-based lidar, (2) quantify the strength and variability of O_3-NO_2 and O_3-HCHO relationships across diurnal and seasonal timescales and assess how these relationships vary across surface, column, and remote sensing observational platforms, and (3) investigate nonlinear O_3 formation by evaluating how O_3 sensitivity to its precursors changes diurnally and seasonally. In doing so, this study applies Pandora-derived HCHO columns, lidar-constrained boundary layer normalization of satellite retrievals, and lagged O_3-HCHO analysis in a semi-arid urban environment where such observations have been largely absent. This study provides the first diurnal and seasonal analysis of O_3-precursor relationships in Tucson, advances understanding of the mechanisms controlling O_3 variability in Arizona's Sun Corridor and establishes a transferrable framework for ground-based validation of TEMPO in semi-arid regions where sparse measurements, complex terrain, and dust represent persistent observational challenges (Sorooshian et al., 2024; Lorente et al., 2017).

https://doi.org/10.5194/egusphere-2026-3397
Preprint. Discussion started: 29 July 2026

The remainder of this paper is organized as follows. Section 2 describes the study site, instrumentation, and analysis methods. Sect. 3 presents results organized around the diurnal and seasonal variability of NO_2, HCHO, and O_3, followed by an analysis of O_3-precursor relationships including meteorological and chemical drivers, evaluation of TEMPO and Pandora column observations normalized by lidar-derived PBLH, and lagged O_3-HCHO relationships. Section 4 provides conclusions and implications for O_3 air quality management in semi-arid urban environments.

2 Methods

2.1 Site Descriptions

For this study, we utilize three monitoring sites across Tucson, Arizona's urban areas and city center (Fig. 1). The Children's Park (CP) site (32.295°N, 110.982°W; AQS Site ID: 04-019-1028), operated by the U.S. EPA AQS as a National Core (NCore) monitoring station, is located in northwestern Tucson. The 22nd and Craycroft (C22) site (32.204°N, 110.878°W; AQS Site ID: 04-019-1011), also operated by U.S. EPA AQS, is located in southeastern Tucson. The Pandora spectrometer, hosted by NASA's Pandora Global Network (PGN), is located in central Tucson atop the Gould-Simpson building at the University of Arizona (32.230°N, 110.955°W) at an altitude of 40 m. Each site is located within a shared ecological and anthropogenic landscape characterized by the Arizona Upland subdivision of the Sonoran Desert and surrounding urban development (Homer et al., 2020; Sorooshian et al., 2024). Figure 1 shows that each site utilized within the study is within the built-up land class. CP and C22 are located adjacent to shrubland land cover classes, whereas PGN is located in a denser built-up area.

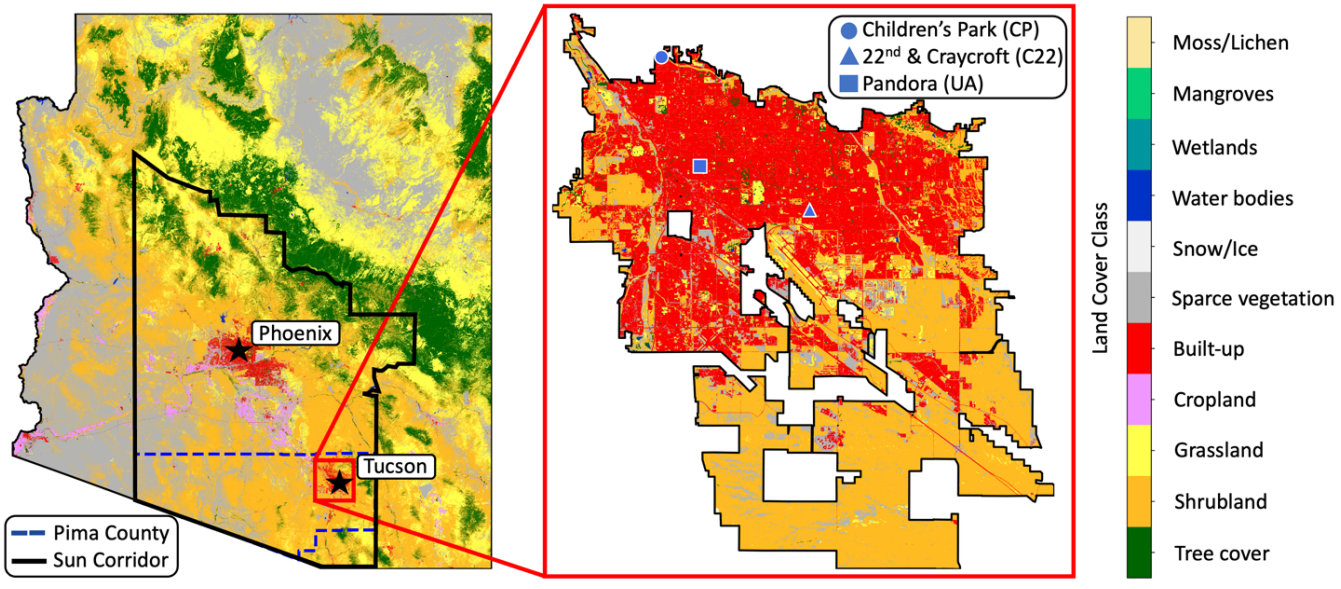

https://doi.org/10.5194/egusphere-2026-3397
Preprint. Discussion started: 29 July 2026

Figure 1: Land cover classification of the state of Arizona and the city of Tucson. Pima County is outlined with a blue dashed line, and Arizona's Sun Corridor is outlined with a blacked dashed line. Children's Park (CP), 22nd & Craycroft (C22), and Pandora (PGN) are shown on the inset map with a blue circle, triangle, and square respectively.

2.2 Instruments

2.2.1 U.S. EPA Air Quality System (AQS)

Surface O_3 and NO_2 observations were obtained from the United States Environmental Protection Agency (U.S. EPA) Air Quality System (AQS) database for the CP monitoring site in Tucson, Arizona, spanning 01 January 2024, through 01 October 2025. Instruments report hourly measurements 24 hours per day. O_3 observations were filtered to include only measurements bearing the XS qualifier, indicating traceability to the EPA Standard Reference Photometer (SRP) scale using the Hearn (1961) O_3 absorption cross-section value of 308.32 atm^{-1} cm^{-1}. It is noted that the EPA updated this cross-section value to 304.39 32 atm^{-1} cm^{-1} beginning 01 January 2025, which may introduce a small systematic offset between 2024 and 2025 O_3 data. NO_2 observations were filtered to remove all adverse qualifiers. Unlike O_3, no standard reference was provided for NO_2. Outliers were additionally removed if they exceeded three times the median absolute deviation (MAD) of the entire data (Leys et al., 2013). Instrument specifications and measurement methods are summarized in Table 1.

Table 1: Surface O_3 and NO_2 instrumentation at the EPA Air Quality System (AQS) monitoring sites in Tucson, Arizona.

Pollutant	Site	Instrument	Measurement Method	Detection Limit
NO_2	22nd & Craycroft (C22)	Teledyne T500U	CAPS spectroscopy[a]	0.04 ppb
NO_2	Children's Park (CP)	Thermo Model 42	Chemiluminescence[b]	1.0 ppb
O_3	22nd & Craycroft (C22)	Thermo Model 49	UV photometry[c]	0.005 ppb
O_3	Children's Park (CP)	Thermo Model 49	UV photometry[c]	0.005 pbb

[a] Federal Equivalent Method (FEM), EQNA-0514-212

[b] Federal Equivalent Method (FEM), RFNA-1289-074

[c] Federal Equivalent Method (FEM), EQOA-0880-047

Note: O_3 measurements are reported in ppm in the AQS dataset and converted to ppb.

2.2.2 Pandora

Tropospheric column and surface retrievals of NO_2 and HCHO were obtained from a Pandora spectrometer as part of NASA's Pandonia Global Network (PGN). Pandora instruments measure direct solar irradiance and sky-scattered radiance in the UV–visible spectral range. Total columns are retrieved using direct-sun Differential Optical Absorption Spectroscopy (DOAS), in which narrow-band absorption features in the measured spectra are fit to reference cross-sections to determine slant column densities that are subsequently converted to vertical columns using geometric air mass factors (Herman et al., 2009).

https://doi.org/10.5194/egusphere-2026-3397
Preprint. Discussion started: 29 July 2026

Tropospheric column and surface concentrations estimates are retrieved using Multi-Axis DOAS (MAXDOAS) sky-scanning observations (Rawat et al., 2025; Cede et al., 2025). Measurements are recorded approximately every 1-2 minutes under clear-sky conditions. The effective horizontal sensitivity is typically a few kilometers near local noon and increases to approximately 10-20 km at larger solar zenith angles, with vertical sensitivity spanning the troposphere above the instrument (Cede et al., 2025). Pandora Level 2 data quality flags were used to filter retrievals. Flags 0 and 10 correspond to high-quality retrievals, while flags 1 and 11 correspond to medium-quality retrievals where at least one diagnostic exceeded the primary quality threshold, for which the reported uncertainty may slightly underestimate the true uncertainty (Cede et al., 2025). Retrievals with low-quality or unusable flags were excluded. Products used in this analysis include NO_2 and HCHO tropospheric columns and surface concentration estimates, collocated using the two nearest grid cells of the Gould-Simpson building.

2.2.3 TEMPO

Tropospheric NO_2 and HCHO retrievals were obtained from the Tropospheric Emissions: Monitoring of Pollution (TEMPO) geostationary spectrometer (Zoogman et al., 2017). In this study we use the Level 3 gridded products for NO_2 and HCHO (DOI: 10.5067/IS-40e/TEMPO/NO_2_L3.003 and 10.5067/IS-40e/TEMPO/HCHO_L3.003), which aggregate Level 2 retrievals from a full scan cycle and map them onto a regular latitude-longitude grid (Nowlan et al., 2025). Key specifications of the TEMPO instrument and Level 3 data products are summarized in Table 2.

Table 2: TEMPO instrument and data specifications used in this study.

Property	Specification
Instrument type	UV-visible grating spectrometer
Spectral range	293-494 nm, 538-741 nm
Spectral resolution	~0.6 nm
Native pixel resolution (Level 2)	~2.0 km x 4.75km (nadir)
Level 3 grid resolution	0.02° x 0.02°
Temporal resolution	~1 hour daytime sampling
Retrieved species	NO_2: vertical_column_troposphere; HCHO: vertical_column

To compare TEMPO retrievals with ground-based measurements, TEMPO grid cells were paired with monitoring locations in Tucson, Arizona, including Pandora and CP sites. For each site, the nearest TEMPO grid cell was extracted to represent the satellite column of NO_2 and HCHO at that location. Satellite and ground-based data were matched temporally by pairing TEMPO timeseries of the selected grid cell with both Pandora and CP data, retaining only pairs sampled within 30 minutes of

https://doi.org/10.5194/egusphere-2026-3397
Preprint. Discussion started: 29 July 2026

one another. The values were then floored to their shared hour. These paired datasets were used for subsequent correlation and sensitivity analyses.

Biases between TEMPO and Pandora column retrievals were evaluated at the PGN site using the satellite-ground observation pairs described above. For each dataset pair, bias was calculated as

$$Mean\ Bias = mean(X_{TEMPO} - X_{PGN}) \quad (1)$$

where X_{TEMPO} represents the TEMPO column retrieval extracted from the nearest grid cell to the PGN site and X_{PGN} represents the corresponding Pandora column retrieval within the matching time window.

2.2.4 Ceilometer

PBLH were derived using the ceilometer observations from the Lufft CHM15k instrument, located at the C22 site of the Unified Ceilometer Network (UCN; https://www.ucn-portal.org/). Key technical specifications of the ceilometer are summarized in Table 3. Raw backscatter signals were both range-corrected and quality flagged before their upload to the Unified Ceilometer Network server. The attenuated backscatter (β) profiles were averaged on 10-minute windows and a 50 m vertical smoothing interval. Only heights above 100 m were used to reduce noise contamination in the near-surface signal.

The PBLH was calculated using the aerosol backscatter gradient method based on Vaisala Corporation algorithm, similar to the method used in Caicedo et al. (2017), however, modified to adapt for Lufft CHM15k instrument (Wiegner and Geiß, 2012). PBLH values were considered where negative β gradients satisfied both a minimum absolute change of 5×10^{-3} m^{-1} sr^{-1} and a minimum 10% relative decrease in backscatter within the adjacent level. The lowest altitude which satisfied both these criteria was chosen as the PBLH, assuming that the vertical profile of aerosols at the near surface is approximated as the depth of turbulent mixing (Stull, 2012; Siebert et al., 2000). Moreover, the PBL was given an upper limit of 300 m within two hours after sunrise, such that misidentification of the residual capping inversion would be mitigated. Lastly, the retrieved PBLH values were visually inspected, with spurious values corrected or removed, and retrievals affected by cloud contamination were removed if there existed a strong positive gradient in the attenuated backscatter (Caicedo et al., 2017).

Table 3: Technical specifications of the Tucson ceilometer used for boundary layer retrieval.

Latitude	Longitude	Elevation	Vertical resolution	Temporal Resolution	Wavelength
32.20° N	110.87° W	788 m	10 m	16 s	1064 nm

The PBLH varies from a few hundred meters to a few kilometers during the day, which significantly alters the extent of pollutants mixing (Ayazpour et al., 2023; Du et al., 2020; Foskinis et al., 2024; Jin et al., 2022; Su et al., 2018). Here, the

https://doi.org/10.5194/egusphere-2026-3397
Preprint. Discussion started: 29 July 2026

ceilometer-derived PBLH is used to normalize the column observations of HCHO and NO_2 by dividing the PGN and TEMPO column measurements by the PBLH and thereby enabling a fair comparison with measurements that represent surface concentrations (Souri et al., 2023; Valin et al., 2015; Valin et al., 2011).

2.3 Correlations

To quantify O_3-precursor relationships, Pearson and Spearman correlation coefficients were calculated for O_3-NO_2 and O_3-HCHO pairs across surface, column, and satellite datasets. These pairs were constructed following the procedures described in Sect. 2.2.1-2.2.3, including pairs from U.S. EPA AQS surface measurements, PGN column retrievals, and TEMPO satellite observations. The Pearson correlation coefficient is defined as

$$r = \frac{cov(X,Y)}{\sigma_X \sigma_Y} \quad (2)$$

where $cov(X,Y)$ is the covariance of variables X and Y and σ_X and σ_Y are their respective standard deviations. The Spearman correlation coefficient is defined as

$$\rho = \frac{cov(rank(X),rank(Y))}{\sigma_{rank(X)}\sigma_{rank(Y)}} \quad (3)$$

where $rank(X)$ and $rank(Y)$ are the ranked values of X and Y and $\sigma_{rank(X)}$ and $\sigma_{rank(Y)}$ are their standard deviations, respectively. Pearson correlations capture linear relationships while Spearman correlations provide a non-parametric measure robust to non-normal distributions and nonlinear relationships (Wilcox, 2016).

2.4 Lagged O_3-HCHO Correlations

To account for the photochemical timescale associated with O_3 production from VOC precursors, lagged O_3-HCHO correlation analyses are performed. Surface O_3 does not respond instantaneously to changes in its precursors, but rather the oxidation of VOCs produces HCHO as an intermediate product. The subsequent formation of O_3 occurs over timescales of hours depending on NO_x availability, photolysis rates, and meteorological conditions (Finlayson-Pitts and Pitts, 1993; Qu et al., 2021; Volkamer et al., 2005). Standard concurrent correlations between O_3 and HCHO may therefore underestimate the true strength of the O_3-precursor relationship by neglecting this photochemical delay. To capture this, O_3 observations were paired with HCHO observations preceding the O_3 observations by zero to 12 hours. This lagged pairing represents the chemical production timescales of VOC oxidation and O_3 formation under typical boundary layer conditions in a semi-arid urban environment. Spearman correlation coefficients are calculated for each lagged-hour case following the procedure described in Sect. 2.3. Across all 13 lagged-hour cases, the correlation coefficients of greatest magnitude for each month and hour pair were retained for analysis. This is used to identify the characteristic photochemical delay between VOC oxidation and surface O_3 formation.

https://doi.org/10.5194/egusphere-2026-3397
Preprint. Discussion started: 29 July 2026

3 Results and Discussion

3.1 Seasonal and diurnal variability

Seasons are defined following prior studies related to surface O_3 in Arizona (e.g., Greenslade et al., 2024) as: March-May (MAM) for spring, June (J) for dry-summer, July-August (JA) for monsoon-summer, September-November (SON) for fall, and December- February (DJF) for winter. Times of day are grouped as morning (08:00-11:00 local time [LT]), afternoon (12:00-15:00 LT), and evening (16:00-19:00 LT), corresponding to the daylight hours over which Pandora and TEMPO retrievals are available and during which photochemical activity drives O_3 production and precursor variability.

3.1.1 NO_2 variability

Surface NO_2 shows a similar seasonal cycle across sites and instruments, with maxima in the winter (11.1 ppb: CP, see Table 1) and minima throughout spring and dry summer (0.9 ppb: CP) as shown in Fig. 2(a) and Table 4. This pattern is consistent with reduced photochemical loss and a lower PBLH in winter, as well as an increase in photolysis and mixing during the summer months (Monks et al., 2015). There is a reduction of month-to-month variability in PGN column retrievals compared to those of surface observations, with median relative changes of 24% and 9% month to month for CP and PGN column, respectively. The observed shift in the seasonal cycle suggests that the column retrievals are more sensitive to regional-scale processes and background conditions than that to near-surface emissions alone (Lamsal et al., 2008; Harkey and Holloway, 2024). This reduced variability is consistent with the smoothing effect of vertical integration, thus resulting in a muted seasonal cycle (Harkey and Holloway, 2024).

https://doi.org/10.5194/egusphere-2026-3397
Preprint. Discussion started: 29 July 2026

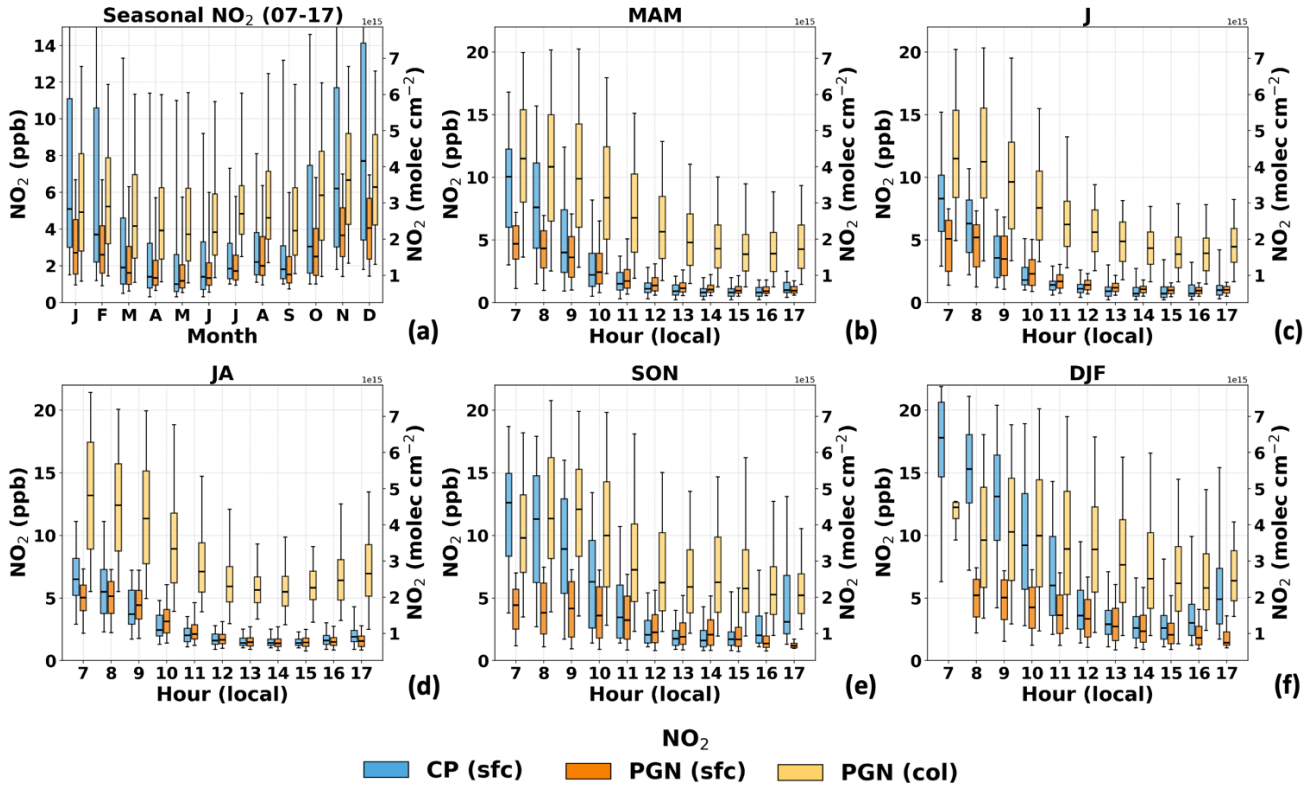

Figure 2: Seasonal and diurnal variability of NO_2 across surface and column observations in Tucson, Arizona. (A) Monthly median NO_2 concentrations across all sites and platforms for the full study period (2024–2025), shown for daylight hours (07:00–17:00 LT). Seasonal median NO_2 diurnal cycles are shown for (B) spring (MAM), (C) dry summer (J), (D) monsoon summer (JA), (E) fall (SON), and (F) winter (DJF). Box plots show the median (center line), interquartile range (IQR; box), and 1.5×IQR (whiskers). Colors indicate CP surface (blue), PGN surface (orange), and PGN column (yellow) observations. Units for surface observations are ppb and for column retrievals are 10^{15} molecules cm^{-2}.

Table 4: Seasonal median ± IQR summary for NO_2 across hours and observations.

Hours	Site	MAM	J	JA	SON	DJF	Units
8:00-11:00	CP	3.1 ± 5.1	2.5 ± 3.5	3.2 ± 2.6	6.6 ± 8.4	11.1 ± 8.8	ppb
8:00-11:00	PGN sfc	2.6 ± 2.9	2.4 ± 2.6	3.3 ± 2.8	3.6 ± 4.0	4.3 ± 3.4	ppb
8:00-11:00	PGN col	3.2 ± 2.7	3.1 ± 2.3	3.5 ± 2.3	3.7 ± 2.8	3.6 ± 2.8	10^{15} molec cm^{-2}
8:00-11:00	TEMPO @ CP	3.4 ± 2.5	3.3 ± 1.8	3.4 ± 1.9	3.6 ± 2.9	4.5 ± 3.0	10^{15} molec cm^{-2}
8:00-11:00	TEMPO @ PGN	3.6 ± 2.5	3.5 ± 2.2	3.9 ± 2.5	3.9 ± 3.2	4.2 ± 3.0	10^{15} molec cm^{-2}

https://doi.org/10.5194/egusphere-2026-3397
Preprint. Discussion started: 29 July 2026

12:00-15:00	CP	0.9 ± 0.8	0.9 ± 0.8	1.5 ± 0.6	1.7 ± 1.3	2.9 ± 2.3	ppb
12:00-15:00	PGN sfc	1.1 ± 0.7	1.11 ± 0.6	1.5 ± 0.7	2.0 ± 1.9	2.5 ± 2.4	ppb
12:00-15:00	PGN col	1.8 ± 1.4	1.8 ± 1.0	2.2 ± 0.9	2.3 ± 1.9	2.8 ± 2.3	10^{15} molec cm^{-2}
12:00-15:00	TEMPO @ CP	1.9 ± 1.4	2.2 ± 1.3	2.7 ± 1.3	2.5 ± 1.7	2.6 ± 2.1	10^{15} molec cm^{-2}
12:00-15:00	TEMPO @ PGN	2.2 ± 1.7	2.7 ± 1.7	3.2 ± 1.7	2.6 ± 2.0	2.6 ± 2.1	10^{15} molec cm^{-2}
16:00-20:00	CP	1.6 ± 2.3	1.5 ± 2.0	2.4 ± 2.0	4.35 ± 7.0	6.5 ± 8.8	ppb
16:00-20:00	PGN sfc	0.9 ± 0.5	1.0 ± 0.5	1.5 ± 0.8	1.3 ± 0.7	1.8 ± 1.4	ppb
16:00-20:00	PGN col	1.6 ± 1.1	1.7 ± 0.9	2.6 ± 1.3	2.1 ± 1.2	2.3 ± 1.6	10^{15} molec cm^{-2}
16:00-20:00	TEMPO @ CP	1.9 ± 1.46	2.2 ± 1.6	3.0 ± 2.5	2.6 ± 2.1	2.2 ± 1.5	10^{15} molec cm^{-2}
16:00-20:00	TEMPO @ PGN	2.5 ± 2.0	2.9 ± 1.9	3.4 ± 2.3	3.0 ± 1.8	2.2 ± 1.5	10^{15} molec cm^{-2}

In regard to the diurnal structure of NO_2, concentrations are consistent with prior studies such that NO_2 peaks during the morning rush hour, and declines as NO_2 undergoes photolysis in the late morning and afternoon (Jin et al., 2025; Greenslade et al., 2024), as shown in Fig. 2(b-f). The morning variability of NO_2 is much stronger in the early fall and winter as compared to late spring and summer, stemming from the photolysis rate increasing in the warmer months (Finlayson-Pitts and Pitts, 1993). After declining to near minimum concentration in the early afternoon, NO_2 remains relatively stable due to photolytic destruction and strong atmospheric mixing and dilution. This effect is especially apparent in the dry and monsoon summers where concentrations do not rise again until the evening, unlike winter where concentrations begin to rise in the mid-afternoon. As NO_2 concentrations begin to increase once again, they coincide with both the evening rush hour and the reduction of sunlight driving photolysis (Jin et al., 2025; Greenslade et al., 2024). CP NO_2 concentrations are greater than those of PGN surface in the evening for every season, resulting from the smoothing effect of PGN's surface approximation of the column retrievals (Harkey and Holloway, 2024; Knepp et al., 2015). Overall, the seasonal and diurnal variability of NO_2 across surface and column observations reflects the combined influence of photochemical activity, boundary layer dynamics, and emission patterns, with column observations capturing a smoother, regionally integrated signal compared to the more emission-sensitive surface measurements.

3.1.2 HCHO variability

HCHO shows a distinct seasonal cycle across surface and column observations, with maxima during monsoon summer (JA) (4.5 ppb: PGN, 08:00-11:00 LT) and minima during winter (DJF) (2.05 ppb; PGN, 16:00-20:00), as shown in Fig. 3(a) and Table 5. This pattern is opposite to that of NO_2 and is consistent with enhanced photochemical production and biogenic VOC emissions during the warm and humid monsoon months, when vegetation activity, solar radiation and precipitation are at their peak. The winter minimum reflects the suppression of photochemical HCHO production under reduced solar radiation, lower temperatures, and diminished biogenic VOC emissions during the cold and dry season (Finlayson-Pitts and Pitts, 1993; Monks

https://doi.org/10.5194/egusphere-2026-3397
Preprint. Discussion started: 29 July 2026

et al., 2015). The transition from the dry summer to the onset of the monsoon-summer is associated with a substantial increase in HCHO, with relative changes of 35% at PGN surface and 61% at PGN column, shown in Table 6. In contrast, background (non-monsoon) month-to-month variability is expectedly lower, with average relative changes of 14% and 16% for PGN surface and PGN column, respectively. This results in monsoon-to-background ratios of 2.5 for PGN surface and 3.7 for PGN column, showcasing a monsoon-driven enhancement in HCHO beyond the typical seasonal variability. This enhancement provides evidence of enhanced biogenic VOC emissions and photochemical HCHO production during the North American Monsoon in the Sonoran Desert (e.g., Youn et al., 2013; Sorooshian et al., 2024).

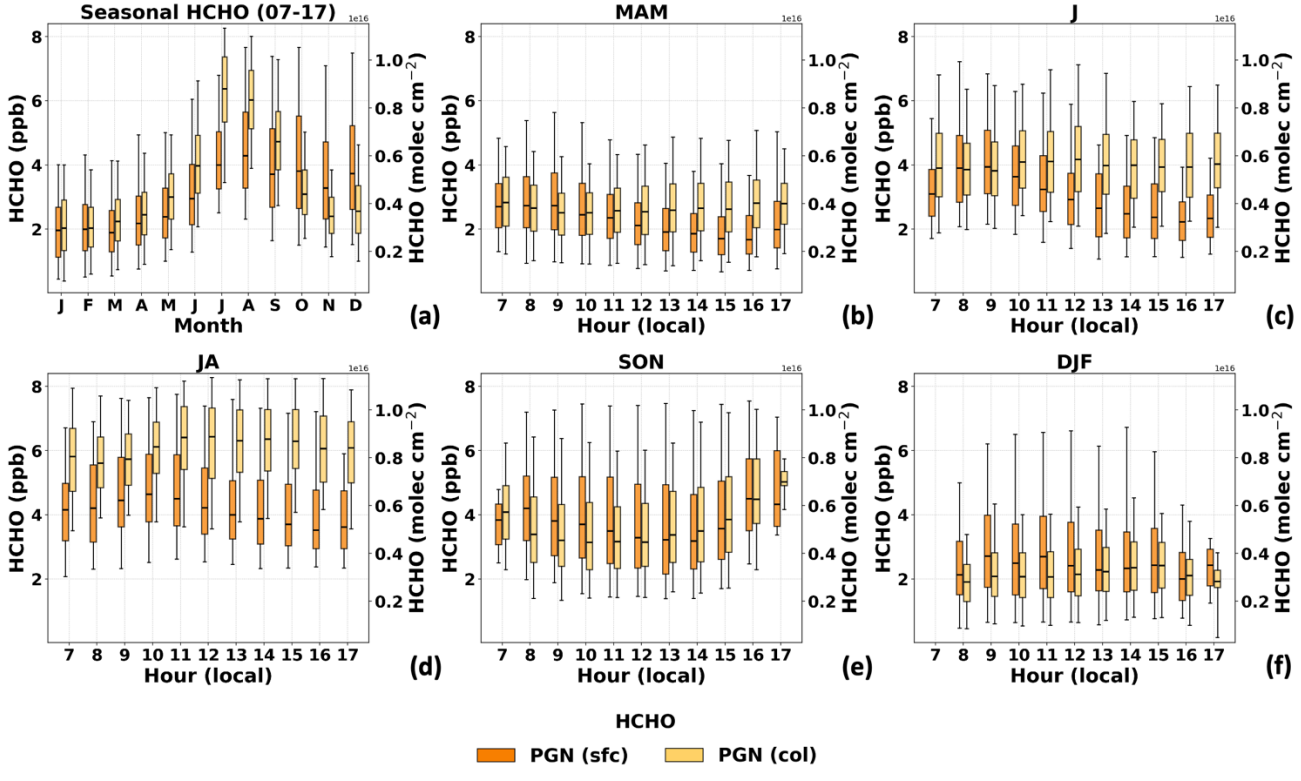

Figure 3: Seasonal and diurnal variability of HCHO across surface and column observations in Tucson, Arizona. (A) Monthly median HCHO concentrations across all sites and platforms for the full study period (2024–2025), shown for daylight hours (07:00–17:00 LT). Seasonal median HCHO diurnal cycles are shown for (B) spring (MAM), (C) dry summer (J), (D) monsoon summer (JA), € fall (SON), and (F) winter (DJF). Box plots show the median (center line), interquartile range (IQR; box), and 1.5×IQR (whiskers). Colors indicate PGN surface (orange) and PGN column (yellow) observations. Units for surface retrievals are ppb and for column retrievals are 10^{16} molecules cm^{-2}.

Table 5: Seasonal median ± IQR summary for HCHO across hours and observations.

https://doi.org/10.5194/egusphere-2026-3397
Preprint. Discussion started: 29 July 2026

Hours	Site	MAM	J	JA	SON	DJF	Units
8:00-11:00	PGN sfc	2.5 ± 1.6	3.6 ± 2.0	4.5 ± 2.2	3.7 ± 2.5	2.6 ± 2.2	ppb
8:00-11:00	PGN col	0.4 ± 0.2	0.6 ± 0.2	0.8 ± 0.2	0.5 ± 0.3	0.3 ± 0.2	10^{15} molec cm^{-2}
8:00-11:00	TEMPO @ PGN	0.6 ± 0.5	0.9 ± 0.6	1.1 ± 0.7	0.8 ± 0.6	0.4 ± 0.5	10^{15} molec cm^{-2}
12:00-15:00	PGN sfc	1.9 ± 1.2	2.6 ± 1.7	4.0 ± 2.0	3.3 ± 2.6	2.4 ± 2.0	ppb
12:00-15:00	PGN col	0.4 ± 0.2	0.6 ± 0.2	0.9 ± 0.3	0.5 ± 0.3	0.3 ± 0.2	10^{15} molec cm^{-2}
12:00-15:00	TEMPO @ PGN	0.6 ± 0.5	1.0 ± 0.7	1.1 ± 0.7	0.8 ± 0.7	0.4 ± 0.6	10^{15} molec cm^{-2}
16:00-20:00	PGN sfc	1.8 ± 1.3	2.3 ± 1.3	3.6 ± 1.9	4.5 ± 2.3	2.1 ± 1.5	ppb
16:00-20:00	PGN col	0.4 ± 0.2	0.6 ± 0.3	0.8 ± 0.3	0.6 ± 0.2	0.3 ± 0.1	10^{15} molec cm^{-2}
16:00-20:00	TEMPO @ PGN	0.3 ± 0.8	0.7 ± 0.9	0.9 ± 0.9	0.7 ± 0.9	0.2 ± 0.7	10^{15} molec cm^{-2}

Table 6: Relative monsoon enhancement of HCHO (June to July) and background (non-monsoon) variability.

Dataset	Monsoon Change	Background Change	Monsoon / Background
PGN sfc	35%	14%	2.5
PGN col	61%	16%	3.7

The diurnal structure of HCHO differs markedly from that of NO_2, with surface concentrations generally increasing and peaking in the morning, consistent with photochemical production from VOC oxidation (Stavrakou et al. 2015; Jin et al., 2025; De Smedt et al., 2015), as shown in Fig. 3(b-f). Morning HCHO variability is most pronounced in the monsoon and dry summers, driven by the combination of high biogenic VOC emissions and intense solar radiation in these seasons. While PGN column shows a distinct seasonal variability, there is minimal diurnal variability in comparison to surface retrieval data, as shown in Fig. 3(b-f). This muted diurnal structure may be partly attributable to the near-balance between HCHO production from VOC oxidation and its rapid photochemical loss via photolysis and OH oxidation, which together maintain HCHO concentrations in a near-steady state during daylight hours (Stavrakou et al., 2015). The smoothing effect of vertical integration further dampens the diurnal signal in column retrievals (Harkey and Holloway, 2024). This is evident through the lack of a distinct HCHO morning peak in PGN columns, whereas the morning peak is present in PGN surface retrievals. The morning peak of HCHO may be attributed to the emissions of anthropogenic VOCs and the accumulation of HCHO under a shallow boundary layer. However, this attribution is challenging due to the multiplicity of sources, including mobile sources (vehicle exhaust), stationary sources (industry), and biogenic sources, as well as the temporal variability of emissions (Borbon et al., 2013). Overall, the seasonal and diurnal variability of HCHO reflects the dominant influence of photochemical production and biogenic VOC emissions, with the monsoon period driving the strongest enhancements and column retrievals providing a regionally integrated view of VOC oxidation that complements the near-surface perspective of surface retrievals.

https://doi.org/10.5194/egusphere-2026-3397
Preprint. Discussion started: 29 July 2026

3.1.3 O_3 variability

Surface O_3, measured at CP, shows a distinct seasonal cycle, peaking during monsoon summer (JA) at 60 ppb and reaching a minimum during winter (DJF) at 23.5 ppb, as shown in Fig. 4(a) and Table 6. The summertime maximum is indicative of enhanced photochemical production driven by increased solar radiation and precursor availability consistent with prior regional studies in Arizona (Ajayi et al., 2025; Parakkat et al., 2025; Betito et al., 2024; Greenslade et al., 2024; Guo et al., 2024; Sorooshian et al., 2024). The wintertime minimum reflects reduced photochemical production under lower solar radiation and enhanced O_3 loss via NO titration (Pusede et al., 2015; Nussbaumer and Cohen, 2020). Notably, O_3 deviates from the broader summertime maximum such that June exhibits lower concentrations than spring, suggesting that the pre-monsoon transition in meteorological conditions, including increased moisture, cloud cover, and vertical mixing, may temporarily suppress photochemical O_3 production prior to the full onset of the monsoon (Guo et al., 2024; Sorooshian et al., 2024).

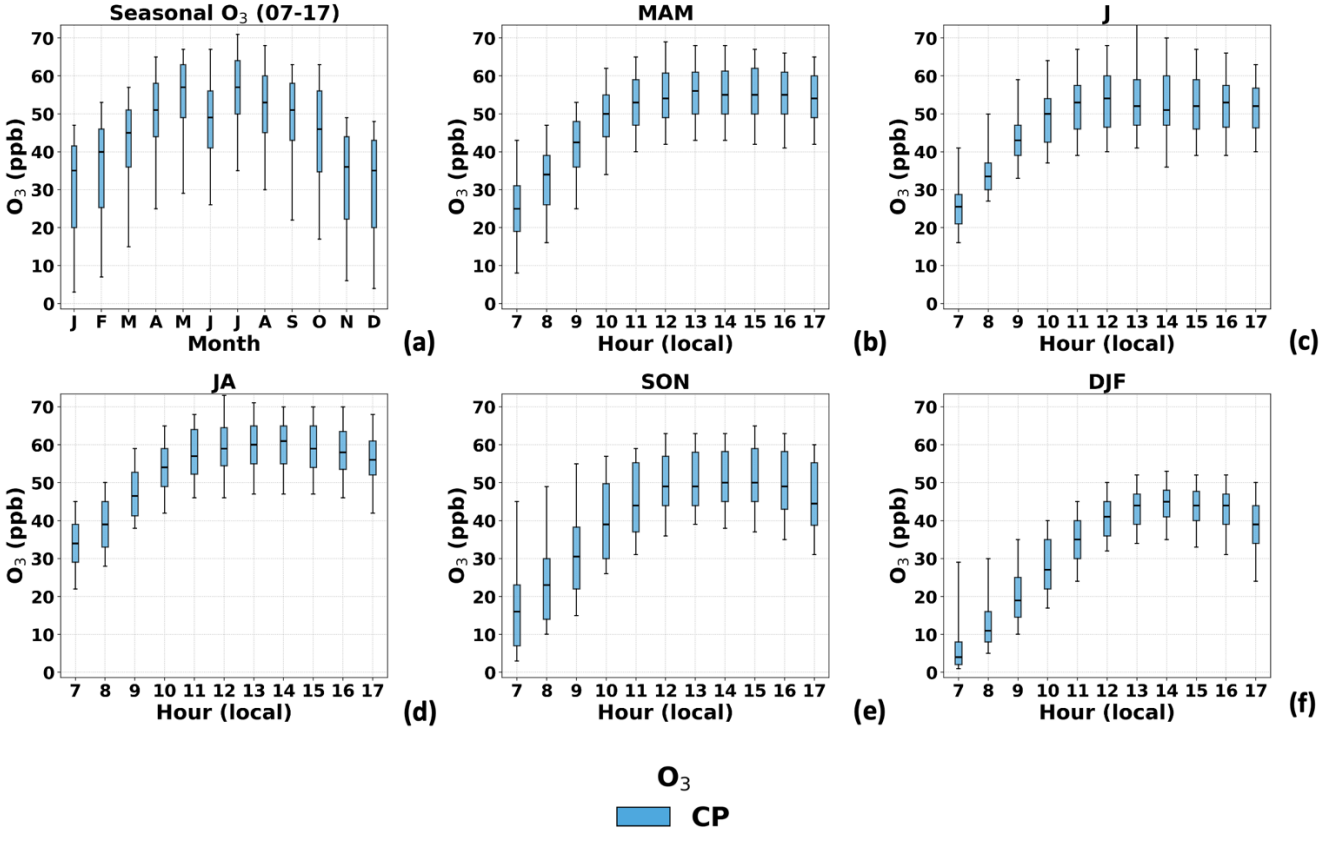

Figure 4: Seasonal and diurnal variability of surface O_3 at CP in Tucson, Arizona. (A) Monthly median O_3 concentrations across one site for the full study period (2024–2025), shown for daylight hours (07:00–17:00 LT). The seasonal median O_3 diurnal cycle is shown for (B) spring (MAM), (C) dry summer (J), (D) monsoon summer (JA), (E) fall (SON), and (F) winter (DJF). Box plots show the median (center line), interquartile range (IQR; box), and 1.5×IQR (whiskers).

https://doi.org/10.5194/egusphere-2026-3397
Preprint. Discussion started: 29 July 2026

Table 7: Seasonal median ± IQR summary for O_3 across hours at CP.

Hours	Site	MAM	J	JA	SON	DJF	Units
8:00-11:00	CP	45 ± 16	45 ± 16	50 ± 14	35 ± 21.8	24 ± 18	ppb
12:00-15:00	CP	55 ± 11	53 ± 13	60 ± 10	49 ± 14	44 ± 8	ppb
16:00-20:00	CP	51 ± 13	49 ± 11	53 ± 13	41 ± 19	33 ± 20	ppb

Like NO_2 and HCHO, the diurnal structure of O_3 reflects the underlying photochemical activity across all seasons, as shown in Fig. 4(b-f) and Table 6. However, in contrast to NO_2, O_3 shows a distinct late morning to afternoon peak, inversely mirroring the diurnal cycle of NO_2 and reflecting the well-known photochemical coupling between these species observed in previous studies for Arizona (e.g., Ajayi et al., 2025; Greenslade et al., 2024). This relationship is examined in detail in Sect. 3.2. Morning O_3 concentrations are lower across all seasons, building through the late morning as photolysis of NO_2 drives O_3 production. O_3 remains relatively persistent in the afternoon, particularly during monsoon summer where concentrations remain above 50 ppb past 17:00 LT. This afternoon persistence reflects the continued balance between photochemical O_3 production and its loss pathways, where sustained precursor availability, high temperatures, and solar radiation maintain O_3 concentrations even as photolysis rates begin to decline in the late afternoon (Pusede et al., 2015; Nussbaumer and Cohen, 2020). This persistence is less apparent in winter, where O_3 peaks sharply in the afternoon (44 ppb: CP, 12:00–15:00 LT) and declines more rapidly, consistent with weaker photochemical activity and a shallower boundary layer during the cold season. The seasonal and diurnal variability of NO_2, HCHO, and O_3 collectively reflect the photochemical and meteorological drivers of O_3 formation in Tucson, with the following subsection examining the consistency between TEMPO and Pandora column retrievals across these seasonal and diurnal timescales.

3.1.4 TEMPO and PGN column retrieval bias

The performance of TEMPO tropospheric column NO_2 and total column HCHO retrievals are assessed through comparison with co-located Pandora column retrievals. Here, biases between TEMPO and PGN are evaluated to provide insight into the limitations of the correlative analysis presented in this study.

https://doi.org/10.5194/egusphere-2026-3397
Preprint. Discussion started: 29 July 2026

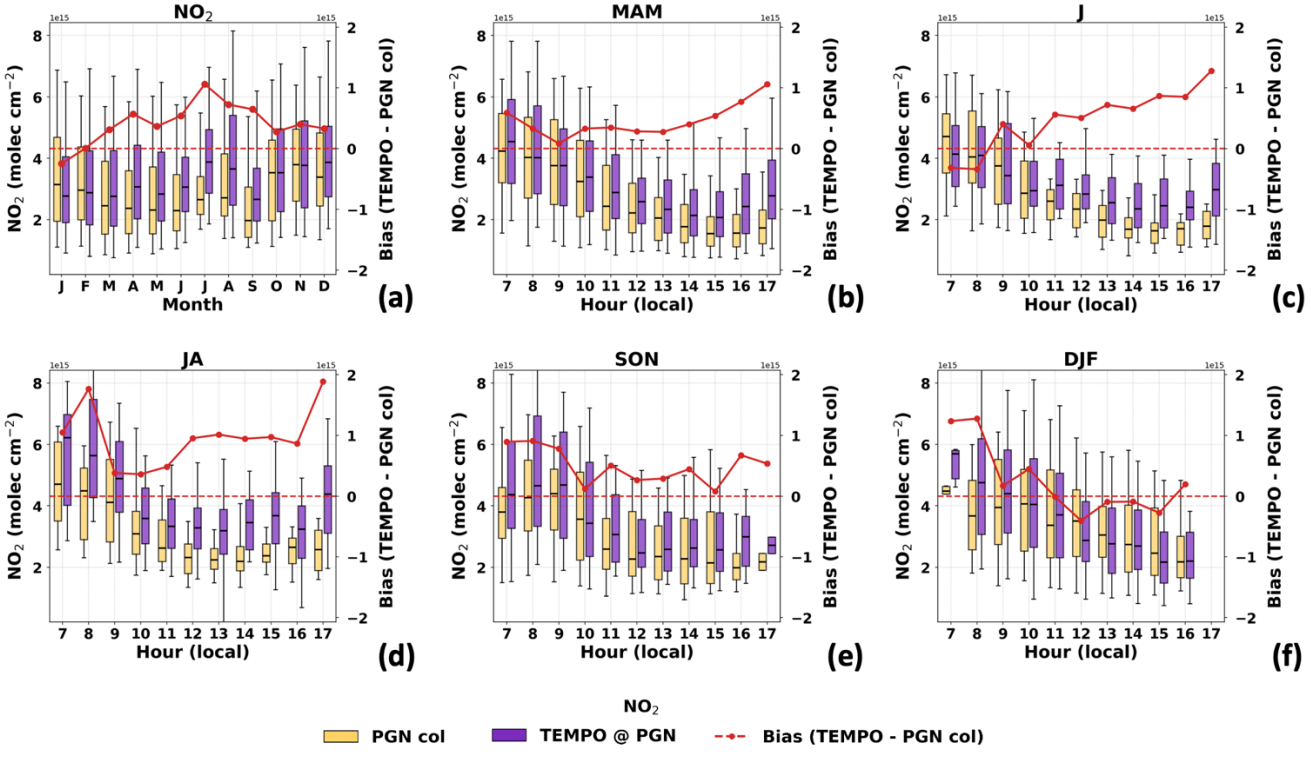

Figure 5: Seasonal and diurnal variability of TEMPO and Pandora tropospheric column NO_2 observations in Tucson, Arizona. (A) Monthly median NO_2 columns for the full study period (2024–2025), shown for daylight hours (07:00–17:00 LT). Seasonal median diurnal cycles are shown for (B) spring (MAM), (C) dry summer (J), (D) monsoon summer (JA), (E) fall (SON), and (F) winter (DJF). Box plots show the median (center line), interquartile range (IQR; box), and 1.5×IQR (whiskers). Colors indicate PGN column (purple) and TEMPO @ PGN (orange) observations. The red dashed line and right axis indicate the mean bias (TEMPO − PGN column) in 10^{15} molecules cm^{-2}. Units for column observations are 10^{15} molecules cm^{-2}.

The observed diurnal and seasonal bias trends between TEMPO and PGN tropospheric columns NO_2 are consistent with known retrieval behavior described in Ghahremanloo et al. (2025), whereby TEMPO underestimates NO_2 at high column densities in the winter months and overestimates at low column densities in the summer months (Fig. 5). The underestimation of NO_2 in the winter reflects a low-boundary layer height and higher solar zenith angles, both of which reduce retrieval accuracy and increase uncertainty (Ghahremanloo et al., 2025). Additionally, early-morning and near-sunset retrievals are less accurate than those obtained in the midday, due to radiative transfer uncertainties at high solar zenith angles and inaccuracies of the simulation of diurnal boundary layer height variations (Ghahremanloo et al., 2025). Generally, however, TEMPO mirrors the diurnal and seasonal trends represented in PGN tropospheric NO_2 retrieval with biases less than $1.5x10^{15}$ molecules cm^{-2}. Notably, as the Pandora instrument is located at an altitude of 738 m above sea level (ASL), additional uncertainties arise

https://doi.org/10.5194/egusphere-2026-3397
Preprint. Discussion started: 29 July 2026

because the PGN does not take into account the vertical distribution of NO_2 below this altitude, whereas TEMPO integrates the entire tropospheric column (Ghahremanloo et al., 2025).

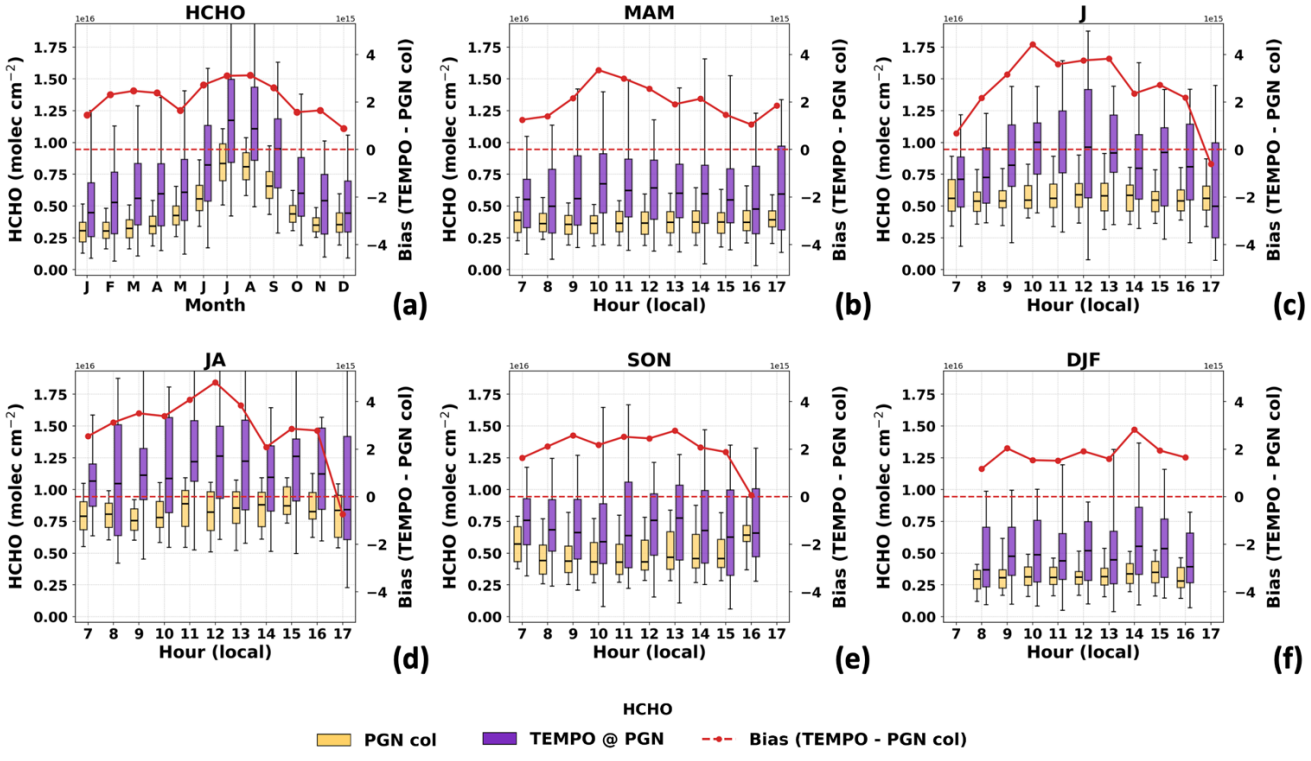

Figure 6: Seasonal and diurnal variability of TEMPO and Pandora total column HCHO observations in Tucson, Arizona. (A) Monthly median HCHO columns for the full study period (2024–2025), shown for daylight hours (07:00–17:00 LT). Seasonal median diurnal cycles are shown for (B) spring (MAM), (C) dry summer (J), (D) monsoon summer (JA), (E) fall (SON), and (F) winter (DJF). Box plots show the median (center line), interquartile range (IQR; box), and 1.5×IQR (whiskers). Colors indicate PGN surface (purple), TEMPO @ PGN (orange), and mean bias TEMPO − PGN column (red dashed line, right axis) in 10^{15} molecules cm^{-2}. Units for column observations are 10^{16} molecules cm^{-2}.

Annually, the biases between TEMPO and PGN total column HCHO retrievals are positive indicating that TEMPO systematically overestimates PGN total column HCHO retrievals across all seasons and hours (Fig. 6). This is in contrast to the NO_2 bias, which shows both positive and negative values depending on the season. Consistent with findings from Rawat et al. (2026) the bias is relatively small in the winter (< $2x10^{15}$ molecules cm^{-2}) and larger during monsoon-summer ($3.5x10^{15}$ molecules cm^{-2}), indicative of higher HCHO concentrations amplifying errors. Moreover, enhanced photochemistry and increased biogenic VOC emissions during the monsoon further increase the potential bias between TEMPO and PGN, particularly as Pandora poorly captures the complexity of the vertical distribution of HCHO during periods of peak emissions

https://doi.org/10.5194/egusphere-2026-3397
Preprint. Discussion started: 29 July 2026

(Rawat et al., 2026). In addition, PGN does not accurately reproduce the vertical shape of the HCHO profile, exhibiting a high bias near the surface and a low bias near the top of the boundary layer (Sebol et al., 2025). As the Pandora instrument at the Gould-Simpson building is located at 738 m ASL, biases between TEMPO and PGN are expected to increase due to the unobserved vertical component of HCHO below instrument level. Diurnally, TEMPO captures an afternoon enhancement of HCHO that PGN does not, likely reflecting Pandora's limited sensitivity to the vertical distribution of HCHO close to the surface (Sebol et al., 2025). While PGN surface retrievals display a consistent diurnal cycle, peaking ahead of TEMPO HCHO in the morning, this study acknowledges the biases inherent in both TEMPO and PGN retrievals as identified from observations and reported in literature (Rawat et al., 2025; Rawat et al., 2026; Sebol et al., 2025).

3.2 O_3-precursor relationships

The seasonal and diurnal variability described in Sect. 3.1 provides the observational foundation for examining O_3-precursor relationships across meteorological, surface, column, and satellite platforms, as presented in the following subsections.

3.2.1 Meteorological drivers

https://doi.org/10.5194/egusphere-2026-3397
Preprint. Discussion started: 29 July 2026

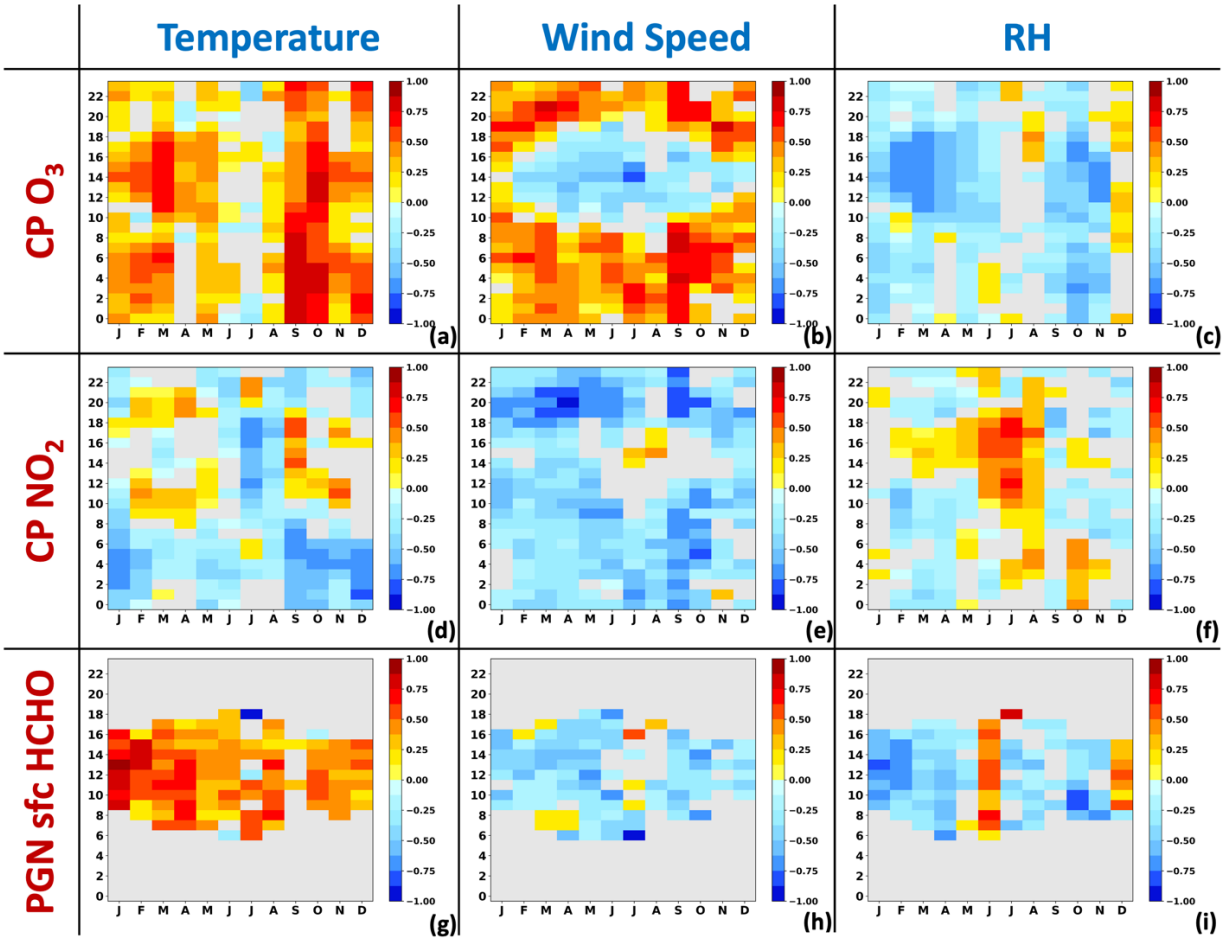

Figure 7: Spearman correlation coefficients ($p < 0.05$) between surface O_3, NO_2, and HCHO and meteorological variables in Tucson, Arizona. Rows indicate the trace gas: CP O_3 (top), CP NO_2 (middle), and PGN surface HCHO (bottom). Columns indicate the meteorological variable: temperature (°C; left), wind speed (m s^{-1}; center), and relative humidity (%; right). Each panel shows the correlation coefficient as a function of month (x-axis) and hour of day (y-axis; local time), with warm colors indicating positive correlations and cool colors indicating negative correlations across a scale of -1 to +1. Correlations not meeting the $p < 0.05$ significance threshold are masked in grey.

Relationships between O_3 and its precursors with meteorology evolve systematically by season, reflecting diurnal and seasonal changes in O_3-precursor relationships and changes in nonlinear chemical behavior (Archibald et al., 2020; Sillman et al., 2002). Figure 7(a-i) illustrates statistically significant ($p < 0.05$) Spearman correlations between O_3, its precursors (rows: O_3, NO_2, HCHO), and meteorology (columns: temperature, wind speed, and relative humidity) where each correlation subplot is

https://doi.org/10.5194/egusphere-2026-3397
Preprint. Discussion started: 29 July 2026

evaluated independently rather than additively (Camalier et al., 2007; Porter and Heald, 2019). The observed relationships are consistent with a non-linear interaction framework, where O_3 responds to combined states of temperature, wind, humidity, and precursors, and the precursors are also dependent upon meteorology (Pusede et al., 2015; Archibald et al., 2020; Porter and Heald, 2019). Thus, there is a physical basis for interpreting the seasonal and diurnal trends of correlations as evidence of non-linear chemistry (Sillman, 2002; Archibald et al., 2020; Nussbaumer and Cohen, 2020; von Schneidemesser et al., 2015; Mirrezaei et al., 2024).

In the late-winter and spring, distinct correlations emerge between chemistry and meteorology. In Fig. 7(a) (O_3-temperature), strong positive correlations are present in the afternoon and evening, while Fig. 7(c) (O_3-RH) exhibits a mirrored negative correlation in the afternoon and evening. Together, these results suggest that O_3 concentrations are highly correlated with radiative conditions, such that warm, dry afternoons enhance concentrations of O_3 and humid conditions suppress it (Stathopoulou et al., 2008; Camalier et al., 2007; Porter and Heald, 2019). This behavior is consistent with the established understanding that O_3 production increases under high-radiation conditions and decreases when photolysis is limited (Fu and Tian, 2019; Fiore et al., 2012; Pusede et al., 2015). Precursor correlations with temperature and RH support this reasoning, such that in Fig. 7(g) (HCHO-temperature), HCHO is strongly positively correlated with temperature, suggesting that the VOC oxidation is also responding directly to meteorological forcing (Wolfe et al., 2016; Nussbaumer and Cohen, 2020).

Moving into the dry summer, the expected positive correlation between O_3 and temperature weakens despite increasing temperatures. This is suggestive of O_3 responding to temperature nonlinearly, reflecting multiple interactions between mixing, precursor availability, and shifts in chemical regime (Sillman et al., 2002; Archibald et al., 2020; Porter and Heald, 2019). As indicated by the strong negative correlation between O_3 and wind speed in the afternoon, there is a competing effect such that favorable conditions for O_3 production (high-temperature) are coinciding with conditions that enhance mixing and dilute concentrations (high-wind speed). Wind speed is itself dependent upon temperature gradients, introducing an additional level of nonlinearity (Camalier et al., 2007). Additionally, as shown in Fig. 7(i), there is a strong positive correlation between HCHO and RH that does not continue into the monsoon summer. Thus, RH in the dry summer may be associated with enhanced oxidation of VOCs while radiation remains sufficient for photochemistry (Chatfield et al., 2010; Wolfe et al., 2016). Overall, the dry summer represents a transitional regime where meteorology influences chemistry through multiple competing interactions, reflecting a shift toward increasingly nonlinear behavior relative to the more temperature-dominant regimes of late winter and spring (Camalier et al., 2007; Fiore et al., 2015).

The most pronounced shifts in O_3, precursor, and meteorology relationships occur during the monsoon summer. Across Fig. 7(a-c), O_3-temperature correlations weaken (-) and those O_3-RH strengthen (+), suggesting that O_3 variability is increasingly defined by the complex meteorological interactions associated with the monsoon (Sorooshian et al., 2024; Ajayi et al., 2025; Guo et al., 2024). The negative correlation between O_3 and wind speeds (-) peaks during this period, reflecting a strong dilution

https://doi.org/10.5194/egusphere-2026-3397
Preprint. Discussion started: 29 July 2026

effect competing with peak O_3 formation. Notably, NO_2-wind speed correlations peak positively during the monsoon, reflecting the role of enhanced monsoonal inflow associated with southerly and easterly winds from the Gulf of California and Mexico in transporting regional NO_2 into Tucson, counteracting local dilution (Betito et al., 2024; Malloy and Cerveny, 2019). As for HCHO, the strong positive (+) correlation with RH becomes negative (-), and correlations with temperature and wind are diurnally highly variable. Given that HCHO nonlinearly depends upon VOC oxidation pathways and its loss via photolysis and OH oxidation, the weakening of these correlations suggests that HCHO concentrations vary nonlinearly with meteorology during monsoon (Wolfe et al., 2016; Archibald et al., 2020). Thus, there is evidence of nonlinear O_3 formation, where O_3 responds to the multiple interactions of meteorology and chemistry rather than being directly tied to a single driver (Pusede et al., 2015; Archibald et al., 2020; Fiore et al., 2015; von Schneidemesser et al., 2015).

Following the monsoon summer and into the fall, Fig. 7(a) shows once again a strong positive correlation between O_3 and temperature throughout the day, suggesting a re-establishment of a more temperature-dominant regime in which photochemistry dominates over other meteorological variables (Fu and Tian, 2019; Porter and Heald, 2019). Notably, the re-emergence of negative O_3-RH correlations in the fall mirrors the pattern observed in late winter and spring, further supporting the interpretation of a temperature-dominant, radiation-controlled photochemical regime (Stathopoulou et al., 2008; Camalier et al., 2007). Moreover, this shift to a more structured behavior, also seen in the late-winter and spring, supports the interpretation that the weak summer correlations reflect a transition to a more nonlinearly dominated regime.

3.2.2 Surface O_3-precursor relationships

The analysis of the relationship of ground-level O_3 and its precursors is based upon co-located observations of O_3 and NO_2 from EPA AQS monitoring site CP as well as HCHO from PGN surface. These datasets provide a direct view of local conditions, especially impacting human health, ecosystem, and agriculture, by representing local photochemical reactions between O_3 and its precursors. Fig. 8 and 9 present Spearman correlations, Pearson correlations, and their absolute differences (|S| - |P|) between CP O_3 and surface NO_2 and HCHO observations, respectively, as a function of month and hour of day. The |S| - |P| difference serves as a diagnostic of nonlinear O_3-precursor behavior, where positive values suggest that Spearman captures stronger relationships than Pearson, reflecting the presence of nonlinear associations. Specifically, O_3-NO_2 relationships at the surface are evaluated using correlations of CP measurements of O_3 and NO_2 (Fig. 8(a-c)), with comparison to correlations of CP O_3 and PGN surface NO_2 (Fig. 8(d-f)), while O_3-HCHO relationships at the surface are evaluated using correlations of CP O_3 and PGN surface HCHO (Fig. 9(a-c)).

Across the surface datasets, the seasonal and diurnal variability of O_3-precursor relationships reveals both the photochemical drivers of O_3 and evidence of nonlinear chemical behavior. In late winter, O_3-precursor behavior is limited by relatively weak photochemistry. In the morning, CP correlations of O_3 and NO_2 (Fig. 8(a-c)) are negative, reflecting potential NO-titration dominant behavior and VOC-limited chemical regimes, where additional contributions of NO_x reduce O_3 concentrations

https://doi.org/10.5194/egusphere-2026-3397
Preprint. Discussion started: 29 July 2026

(Sillman et al., 2002). Moving into the afternoon, O_3-NO_2 correlations increase, but remain negative, suggesting that the system nears a transition in chemical regime, but never fully transitions to NO_x-limited. In contrast, during the same period, O_3-HCHO correlations (Fig. 9(a-b)) are positive in the afternoon, suggesting that, even with limited wintertime radiation, O_3 variability is highly correlated with the oxidation of VOCs (Wolfe et al., 2016; Chatfield et al., 2010). This temporally aligns with strong HCHO-RH correlations, suggesting RH as an influential meteorology-chemistry driver of O_3 production in the absence of strong photochemistry (Chatfield et al., 2010; Wolfe et al., 2016). In semi-arid environments such as the Sonoran Desert, episodic winter precipitation triggers rapid vegetative response as desert plants exhibit short-lived pulses of soil moisture availability (Snyder and Tartowski, 2006). This physiological activation of desert vegetation, including creosote bush and other dominant shrubs, can increase the emissions of biogenic VOCs and their oxidized products including HCHO (Jardine et al., 2010; Wolfe et al., 2016). The resulting increase in VOC availability, even under limited wintertime radiation, can contribute to O_3 variability through enhance VOC oxidation pathways, particularly in the presence of sufficient moisture to sustain photochemical activity. While the contribution of additional VOCs does not necessarily result in substantial increases in O_3 concentrations, they can still contribute to O_3 variability in a potential NO_x-limited chemical regime (Sillman, 2002; Pusede et al., 2015). Therefore, in late winter, O_3 variability transitions from NO-titration-driven suppression in the morning to VOC-influenced variability in the afternoon, with HCHO, serving as the dominant correlate of O_3 for maximized production in the winter.

Transitioning from late winter into spring, photochemistry strengthens due to the increased radiation, and O_3-precursor relationships become more dynamic. Correlations of O_3 and NO_2 (Fig. 8(a-c)) become increasingly positive throughout the afternoon, coinciding with peak O_3 production, suggestive of increasing sensitivity of O_3 formation to NO_x under the increased radiation occurring in the spring. Simultaneously, O_3-HCHO correlations also become increasingly positive, suggesting that the oxidation of VOCs continues to influence O_3 formation into the spring. Consistent with the strong correlations of O_3 to both NO_2 and HCHO, the spring afternoon showcases nonlinearity in the O_3-NO_2 correlation: the difference between Spearman, which captures monotonic non-linear relationships, and Pearson, which captures only linear relationships, is positive, suggesting that nonlinear associations dominate over linear ones. Thus, we classify spring afternoons as periods of particularly non-linear O_3 formation.

https://doi.org/10.5194/egusphere-2026-3397
Preprint. Discussion started: 29 July 2026

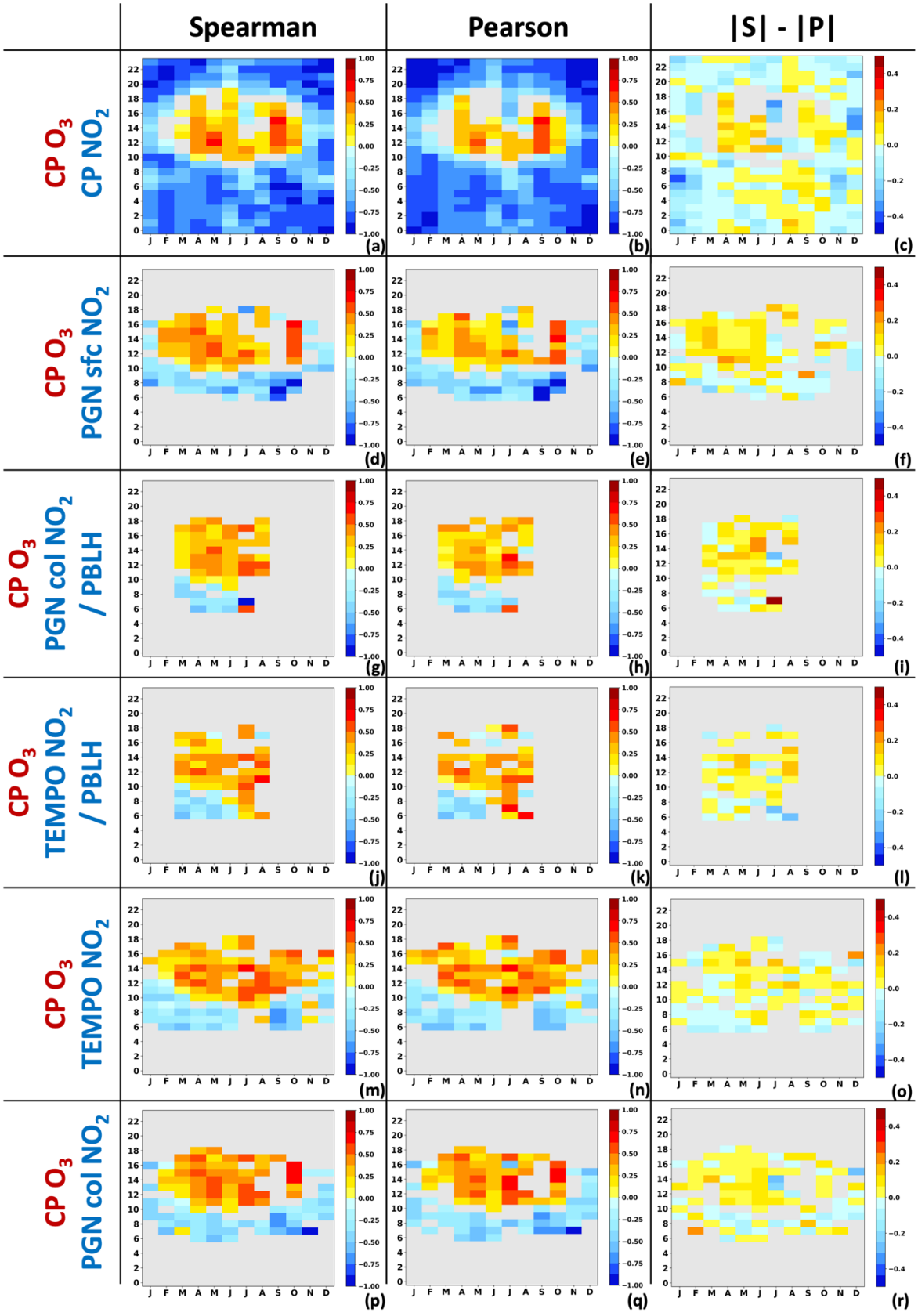

https://doi.org/10.5194/egusphere-2026-3397
Preprint. Discussion started: 29 July 2026

Figure 8: Spearman correlations, Pearson correlations, and their absolute differences (|S| - |P|) between CP O_3 and surface and column NO_2 observations in Tucson, Arizona. Rows indicate the observational pairing: CP O_3 and CP NO_2 (top; panels A-C), CP O_3 and PGN surface NO_2 (second; panels D-F), CP O_3 and PGN column NO_2/PBLH (third; panels G-I), CP O_3 and TEMPO NO_2/PBLH (fourth; panels J-L), CP O_3 and TEMPO NO_2 (fifth; panels M-O), and CP O_3 and PGN column NO_2 (bottom; panels P-R). Columns indicate the correlation metric: Spearman (left), Pearson (center), and |S| - |P| (right). Each panel shows the correlation coefficient as a function of month (x-axis) and hour of day (y-axis; local time). The Spearman and Pearson color scales range from −1 to +1 and the |S| - |P| color scale ranges from −0.5 to +0.5. Correlations not meeting the $p < 0.05$ significance threshold are masked in grey.

In the dry summer, this nonlinear behavior is especially evident. The Spearman correlations of O_3 and NO_2 remain strongly negative in the morning and strongly positive during the afternoon; however, Pearson correlations of O_3 and NO_2 are reduced, resulting in the annual maximum of nonlinear behavior as suggested via the Spearman-Pearson difference. Meanwhile, O_3-HCHO correlations are reduced as compared to the spring, suggesting that the oxidation of VOCs is no longer a substantial indicator of O_3 variability during the dry-summer (Wolfe et al., 2016). While VOC oxidation is strong during the high radiation from the dry summer, it is modulated by meteorology, as illustrated by the strong positive correlation of HCHO-RH in Fig. 7(i).

https://doi.org/10.5194/egusphere-2026-3397
Preprint. Discussion started: 29 July 2026

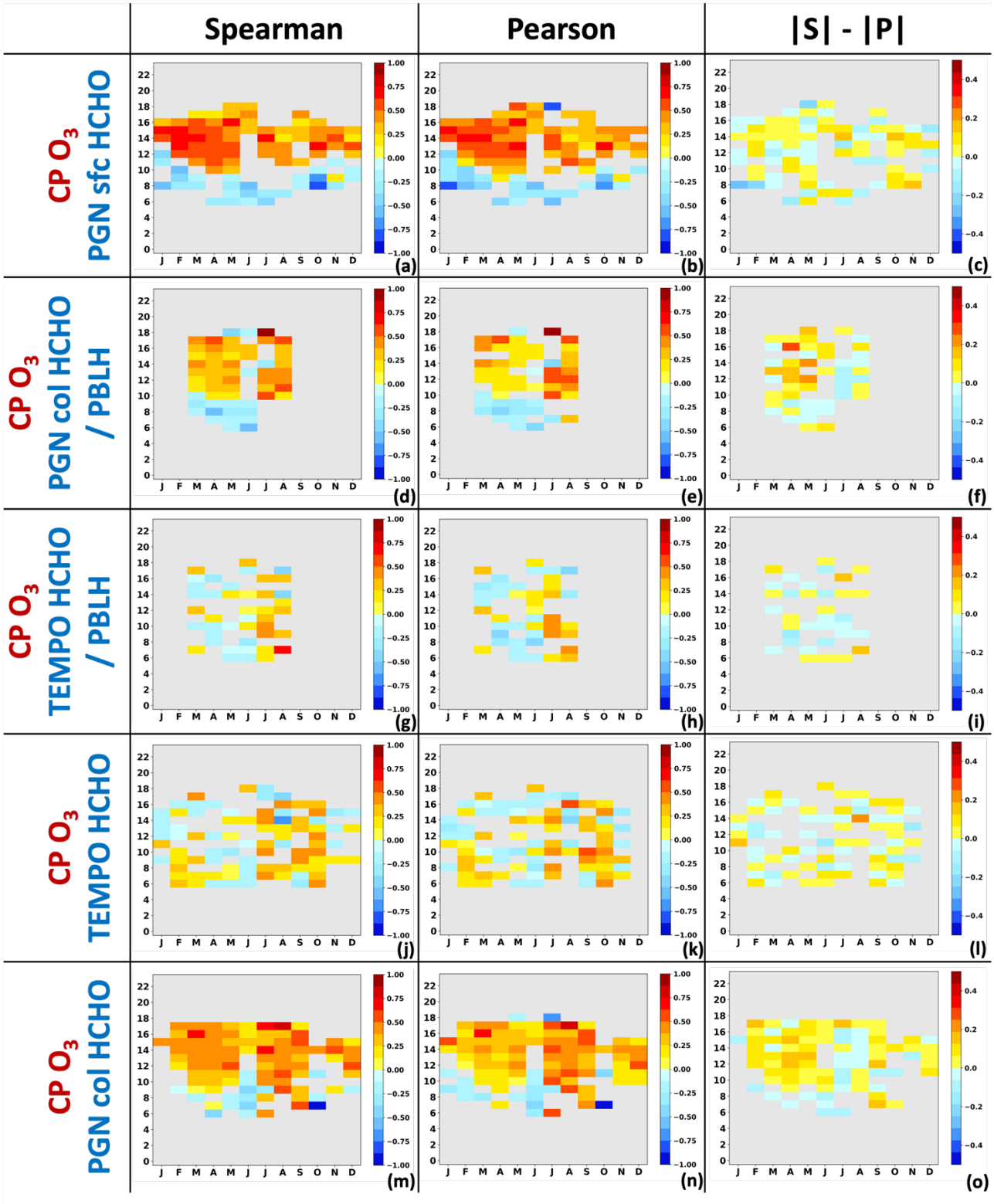

https://doi.org/10.5194/egusphere-2026-3397
Preprint. Discussion started: 29 July 2026

Figure 9: Spearman correlations, Pearson correlations, and their absolute differences (|S| - |P|) between CP O_3 and surface and column HCHO observations in Tucson, Arizona. Rows indicate the observational pairing: CP O_3 and PGN surface HCHO (top; panels A-C), CP O_3 and PGN column HCHO/PBLH (second; panels D-F), CP O_3 and TEMPO HCHO/PBLH (third; panels G-I), CP O_3 and TEMPO HCHO (fourth; panels J-L), and CP O_3 and PGN column HCHO (bottom; panels M-O). Columns indicate the correlation metric: Spearman (left), Pearson (center), and |S| - |P| (right). Each panel shows the correlation coefficient as a function of month (x-axis) and hour of day (y-axis; local time). The Spearman and Pearson color scales range from −1 to +1 and the |S| - |P| color scale ranges from −0.5 to +0.5. Correlations not meeting the $p < 0.05$ significance threshold are masked in grey.

Moving into the monsoon summer, there is a distinct shift in the afternoon and early evening such that O_3-HCHO correlations increase again (Fig. 9(a-c)), suggestive of a second seasonal peak. During the monsoon, biogenic VOC emissions increase, thus increasing the availability of oxidized VOC products and radicals to recycle NO_2 and accordingly form O_3 (Malloy, 2018; Betito et al., 2024) Simultaneously, O_3-NO_2 correlations are still negative in the morning and positive in the afternoon; however, afternoon positive correlations are muted, suggestive of the competing meteorological effects stemming from highly variable correlations of O_3 and its precursors to temperature, wind speed, and RH in the afternoons of the monsoon summer.

Beginning in the fall, as the monsoon retreats, O_3-HCHO correlations weaken and lose their diurnal structure, becoming highly variable throughout the day. Additionally, O_3-NO_2 correlations are maximized in September but are diurnally highly variable throughout the season and into the winter. In the fall, there is a substantial positive correlation between O_3 and temperature while HCHO concentrations remain high, suggesting enhanced photochemistry to shift the chemical regime towards NO_x-limited (Pusede et al., 2015; Greenslade et al., 2024). The late-fall transitions back into the winter seasonal and diurnal variation of surface O_3-precursor relationships.

3.2.3 TEMPO and PGN O_3-precursor relationships

Relative to the surface-based correlations discussed in Sect. 3.2.2, column-based correlations of HCHO and NO_2 with surface based O_3 preserve a similar seasonal and diurnal trend, with the exception of TEMPO HCHO, but with differences in the magnitude and timing (Nawaz et al., 2025). Across each season, O_3-NO_2 correlations from TEMPO and PGN column follow the same diurnal trend (Fig. 8(m-o) and Fig. 8(p-r), respectively), such that weaker or negative correlations occur in the morning and positive correlations dominate in the afternoon, especially in the spring and summer. This agreement across observational contexts suggests that the seasonal and diurnal evolution of O_3-NO_2 relationships are robust across different instrumentation. However, correlations are annually weaker overall, likely reflecting a combination of retrieval biases of TEMPO and PGN column NO_2 as discussed in Sect. 3.1.4, as well as the inherent differences in spatial representativeness and vertical sensitivity between column and surface measurements (Nawaz et al., 2025; Ghahremanloo et al., 2025; Rawat et al., 2025).

https://doi.org/10.5194/egusphere-2026-3397
Preprint. Discussion started: 29 July 2026

A notable exception occurs during the morning of June, where TEMPO HCHO correlations with CP O_3 show no discernible seasonal or diurnal structure. As shown in Fig. 6, TEMPO HCHO biases relative to PGN column are positive throughout the year, with an anomalous afternoon enhancement, inconsistent with both PGN column and PGN surface trends. For PGN column HCHO correlations with CP O_3, positive correlations extend into the morning hours relative to the PGN surface correlations, likely reflecting the reduced sensitivity of column retrievals to localized near-surface variability and greater susceptibility to broader regional influences (Sebol et al., 2025; Tao et al., 2025). Additionally, biases in column HCHO retrievals at high solar zenith angles may contribute to the morning positive correlations (Rawat et al., 2025; Abad et al., 2025).

3.2.4 PBLH-normalized TEMPO O_3-precursor relationships

Column observations of HCHO and NO_2 from TEMPO were normalized by the PBLH following the methods described in Sect. 2.2.4 to model surface concentrations. Success of the proposed method is evaluated by the similarity of seasonal and diurnal trends as well as correlative measures with CP O_3. relative to surface-based observations.

For O_3-NO_2 relationships, TEMPO NO_2 normalized by PBLH (Fig. 8(j-l)) represents surface correlations well in sign and timing with the exception of mornings during the monsoon summer, where correlations are overestimated. In every other season, O_3-NO_2 correlations are muted in the morning such that correlations are underestimated in comparison to surface-based observations. Moreover, nonlinearity in spring afternoons is discernible, showing that the behavior identified in Sect. 3.2.2 persists post-normalization. Generally, seasonal trends are consistent with the surface, supporting its use as a proxy for surface-based measures of NO_2 when true observations are unavailable.

For O_3-HCHO relationships, however, normalization of TEMPO HCHO via PBLH does not recover a discernible seasonal or diurnal structure to represent trends in the surface concentration of HCHO. One possible reason is the neglect of entrainment at the PBL top when normalizing column measurements, particularly during afternoon hours when entrainment rates typically reach a maximum (Caputi et al., 2022; Kaser et al., 2017). Because the entrainment may introduce additional O_3 or its precursors from free troposphere (Caputi et al., 2019; Caputi et al., 2022; Cui et al., 2026; Kaser et al., 2017), this process may contribute to the lack of a discernible diurnal structure of O_3-HCHO relationships. Overall, these uncertainties suggest that HCHO variability is not fully confined to the boundary layer, a key assumption underlying the column normalization approach, and therefore caution is warranted when using PBLH-normalized TEMPO HCHO as a proxy for surface-based measures of HCHO when true observations are unavailable. Future studies using aircraft measurements or fine-resolution modeling are recommended to improve the utilization of PGN column measurements as surface proxy.

Together, these results demonstrate the value of multi-platform observations for characterizing O_3-precursor relationships across spatial and vertical scales. While PBLH-normalized TEMPO NO_2 offers a viable path toward surface-representative NO_2 estimates in regions lacking surface NO_2 measurements, the failure of PBLH normalization for HCHO emphasizes the

https://doi.org/10.5194/egusphere-2026-3397
Preprint. Discussion started: 29 July 2026

importance of dedicated surface HCHO measurements, such as those from PGN, for accurately diagnosing O_3 formation chemistry, particularly in the context of VOC-limited regimes where HCHO serves as a critical precursor indicator (Sillman, 2002; Tao et al., 2022; Jin et al., 2020).

565 **3.2.5 Lagged-HCHO relationships**

While the instantaneous O_3-HCHO correlations discussed in Sect. 3.2.2 and Sect. 3.2.3 characterize the co-variability of surface O_3 and its VOC precursors across diurnal and seasonal timescales, they do not account for the finite photochemical timescale separating VOC oxidation from O_3 formation. Lagged correlations provide a complementary perspective by quantifying the temporal offset between HCHO, an intermediate oxidation product of biogenic and anthropogenic VOCs, and
570 subsequent O_3 production, capturing the photochemical cascade that links VOC emissions to O_3 formation on timescales of hours consistent with VOC oxidation chemistry (Wolfe et al., 2016). Figure 10 presents the maximum Spearman correlation between CP O_3 and HCHO from TEMPO, PGN column, and PGN surface as a function of month and lag hour. Across each observational context, a consistent diurnal lag structure emerges such that lags are smallest near sunrise, increase throughout the afternoon reaching up to 12 hours, and shorten again in the evening. The consistency and differences of this structure across
575 the three platforms provide additional insight into how observational context shapes the diagnosed O_3-HCHO photochemical relationship.

https://doi.org/10.5194/egusphere-2026-3397
Preprint. Discussion started: 29 July 2026

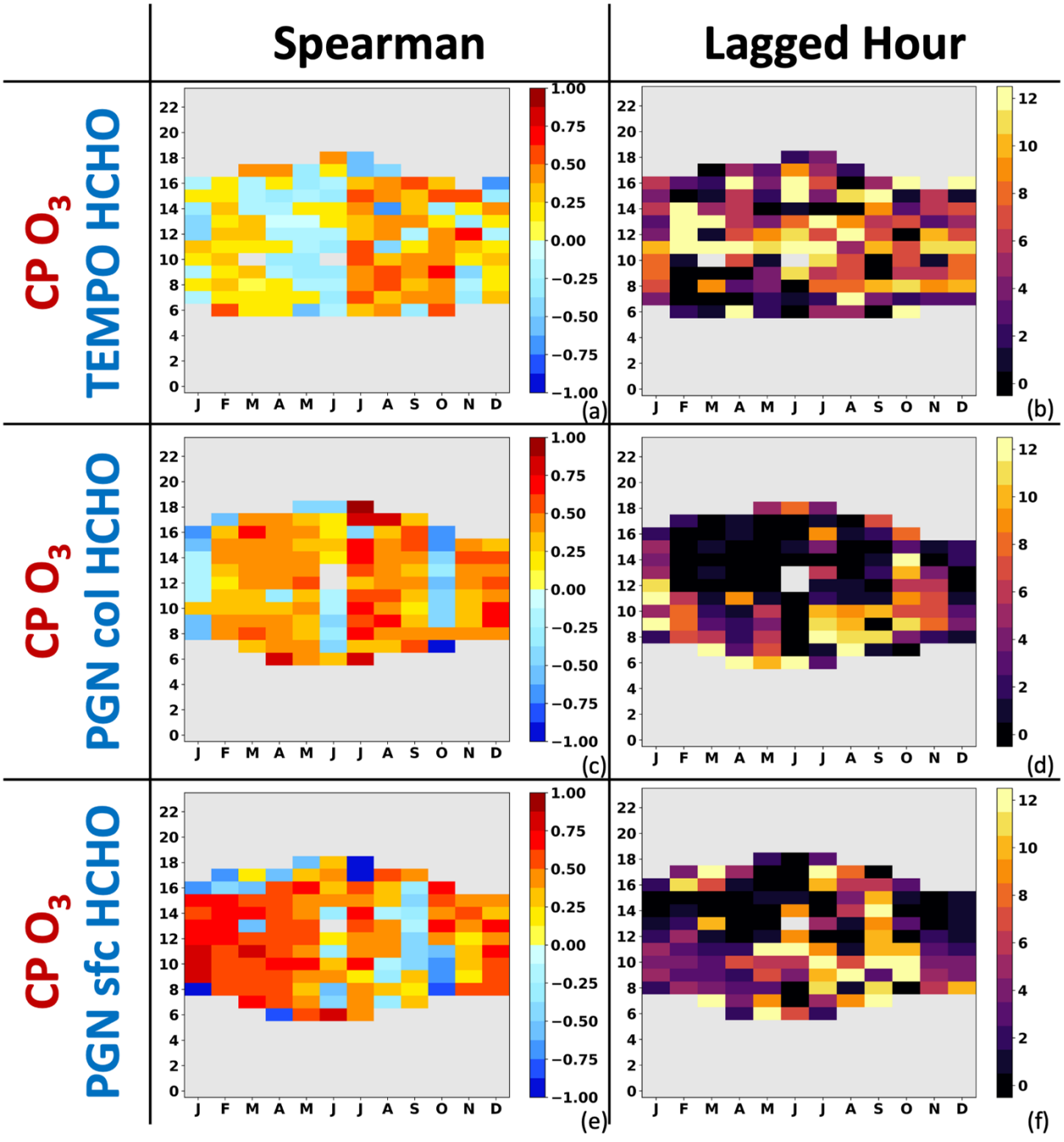

Figure 10: Maximum Spearman correlation coefficients ($p < 0.05$) between CP O_3 and HCHO from three observational contexts. Rows show CP O_3 versus TEMPO HCHO, PGN column HCHO, and PGN surface HCHO respectively. Left-column panels (a, c, e) show the maximum Spearman correlation coefficient across lags of 0-12 hours as a function of month (x-axis) and hour of day (y-

https://doi.org/10.5194/egusphere-2026-3397
Preprint. Discussion started: 29 July 2026

axis; local time), with the color scale ranging from -1 to +1. Right-column panels (b, d, f) show the lag hour associated with the maximum absolute correlation, with the color scale ranging from 0 to 12 hours. Correlations not meeting the $p < 0.05$ significance threshold are masked in grey.

Across three observational contexts, the diurnal lag structure is physically consistent with the daily evolution of photochemistry, such that the oxidation of VOCs produces HCHO prior to the peak O_3 formation, and the time separation increases as photochemistry intensifies with additional radiation throughout the day. The evening decline in lag times may reflect the converse such that as radiation declines, there is a corresponding decline in photolysis and oxidation of HCHO.

In the TEMPO HCHO context, correlations are weakest of the three, with regions of positive correlation occurring in late winter to early spring as well as the monsoon summer to early fall. This likely reflects that TEMPO HCHO represents a column-integrated signal of VOC oxidation rather than a surface-local tracer and may therefore be less responsive to local O_3 variability on the timescales captured by the lag analysis (Wang et al., 2022; Rawat et al., 2026).

In the PGN column HCHO context, the lag structure is similar to that of TEMPO HCHO; however, correlations are substantially stronger with positive maxima in the monsoon summer afternoons and positive correlations in the afternoon of each season, with an additional correlative enhancement in the spring. This shows that lagged correlations of PGN column HCHO to CP O_3, reveal a strong dependence of column HCHO on O_3 formation in the monsoon summer not captured by the instantaneous surface correlations. During the monsoon, enhanced boundary layer mixing may vertically redistribute HCHO in ways better captured by a column measurement than a surface measurement, consistent with the sensitivity of column HCHO retrievals to the full vertical extent of HCHO distribution (Sebol et al., 2025).

In the PGN surface HCHO context, correlations peak in the spring afternoons and decline in the dry summer, missing the monsoon enhancement seen in the PGN column. This is consistent with the non-lagged O_3-HCHO surface relationships discussed in Sect. 3.2.2, suggesting that surface HCHO captures local near-surface VOC oxidation well in spring but is less sensitive to the broader vertical redistribution of HCHO during the monsoon. As a result, surface HCHO is a less reliable indicator of O_3 variability during the monsoon summer, when meteorological processes beyond local surface chemistry become increasingly influential (Betito et al., 2024; Sorooshian et al., 2024).

Across platforms, the lagged O_3-HCHO framework reveals a temporally structured photochemical relationship not apparent in instantaneous correlations, providing physically interpretable evidence of the VOC oxidation cascade driving O_3 formation in Tucson. The seasonal divergence between surface and column contexts during the monsoon demonstrates that both the timing and vertical distribution of VOC oxidation products influence O_3 formation in semi-arid environments, with direct relevance to the interpretation of geostationary HCHO observations for surface O_3 precursor diagnostics.

https://doi.org/10.5194/egusphere-2026-3397
Preprint. Discussion started: 29 July 2026

4 Conclusion

This study presents the first multi-platform diurnal and seasonal analysis of O_3-precursor relationships using TEMPO in a semi-arid monsoon-influenced urban environment, revealing that these relationships are fundamentally shaped by meteorology-chemistry-emissions coupling and are sensitive to the observational context in which they are diagnosed. The North American Monsoon drives a distinct seasonal shift in O_3 precursor dominance, from anthropogenic NO_2 in winter to biogenic VOC oxidation products in summer, with implications for O_3 mitigation strategies that are sensitive to this seasonal transition.

Surface and column observations reveal distinct diurnal and seasonal trends in O_3, NO_2, and HCHO across Tucson, Arizona, with notable differences in the magnitudes and timings of O_3-precursor relationships between observational contexts. Surface NO_2 exhibits ~24% monthly variability and morning peaks driven by local emissions and photochemical loss, whereas PGN column NO_2 exhibits a muted seasonal cycle (~9% monthly variability) stemming from the vertical integration of the measurements and increased sensitivity to background concentrations (Harkey and Holloway, 2024; Lamsal et al., 2008). Despite differences in seasonal variability, diurnal O_3-NO_2 relationships are broadly consistent across observational contexts, with negative correlations in the morning and positive correlations in the afternoon, especially in the spring and summer (Monks et al., 2015). Column correlations of O_3 and NO_2, however, are weaker and less sensitive to O_3 loss by NO titration (Sillman, 2002). In contrast, HCHO shows more pronounced divergence between observational contexts relative to NO_2. Surface HCHO exhibits a diurnal cycle characterized by a morning peak driven by local VOC oxidation, whereas PGN column HCHO lacks a distinct morning peak, reflecting the smoothing effects of vertical integration from column retrievals (De Smedt et al., 2015; Wolfe et al., 2016).

The difference between column and surface HCHO retrievals is illustrated in the O_3-HCHO relationships such that surface correlations are strongest in spring afternoons but weaken during the dry summer, increasing again in the monsoon summer, whereas column HCHO correlations with O_3 show a monsoon enhancement of O_3-VOC coupling not evident in the surface-based O_3-HCHO relationships. This suggests that column measurements capture the vertical redistribution of HCHO during the monsoon summer, whereas surface measurements capture the local influence of VOC emissions (Sebol et al., 2025; Rawat et al., 2025). The PBLH normalization method improves agreement between column-based NO_2 and surface-based O_3 correlations but does not improve agreement for column-based HCHO retrievals, suggesting that HCHO variability may not be fully confined within the boundary layer and may be influenced by additional vertical processes such as entrainment at the top of the PBL (Sebol et al., 2025). These results show that the timing and magnitude of O_3-precursor relationships vary across observational contexts, reflecting differences in sensitivity to local versus regional influences across platforms with varying spatial footprints and vertical sensitivities (Fishman et al., 2008; Verhoelst et al., 2021; Nawaz et al., 2025).

https://doi.org/10.5194/egusphere-2026-3397
Preprint. Discussion started: 29 July 2026

Integrating both surface and column measurements improves characterization of O_3 formation in semi-arid urban environments, suggesting that no single platform alone fully captures O_3-precursor relationships. Moreover, nonlinear O_3 formation is evident through the Spearman-Pearson difference diagnostic, such that nonlinearity is most pronounced in the spring and summer afternoons. During these periods, O_3 sensitivity to its precursors, both NO_2 and HCHO, is highly variable, suggesting a possible transition between VOC- and NO_x-limited chemical regimes (Sillman, 2002; Jin et al., 2020). Nonlinearity is also evident in the distinct lagged structure of O_3-HCHO relationships, consistent with O_3 responding to VOC oxidation on multi-hour timescales. The diurnal evolution of lag times, smallest near sunrise, increasing through the afternoon, and declining in the evening, is physically consistent across all three observational platforms, highlighting the importance of accounting for photochemical timescales in O_3 precursor diagnostics in semi-arid environments (Wolfe et al., 2016).

Accurately diagnosing O_3 formation in semi-arid urban environments requires careful characterization of VOC chemistry, such that HCHO serves as a key, albeit imperfect, component of chemical regime identification (Zhu et al., 2017; Wang et al., 2022). The integration of Pandora, TEMPO, and U.S. EPA AQS observations demonstrates that geostationary satellite retrievals, when combined with surface and ground-based column measurements, provide a more comprehensive characterization of O_3 formation. Transitions in chemical regimes, as evidenced by the variability in O_3-precursor relationships, are dynamic and dependent upon the method of retrieval, suggesting that diagnostics should be evaluated as a function of time and observational context (Archibald et al., 2020; Fiore et al., 2015). The methods developed in this study provide a transferable framework for diagnosing O_3 formation chemistry across observational contexts, with particular relevance to other semi-arid urban environments across the southwestern United States and Mexico where TEMPO provides hourly geostationary observations, and more broadly applicable to regions monitored by current and future geostationary satellite missions.

This study has several limitations. First, HCHO is used in this study as a proxy for VOC reactivity; however, HCHO does not indicate the composition or reactivity of individual VOC species, particularly shorter-lived compounds, but rather reflects the integrated oxidation product of multiple VOC pathways, including biogenic precursors such as isoprene (Wolfe et al., 2016). This limitation is particularly relevant in semi-arid regions such as the southwestern United States, where biogenic emissions can vary rapidly during the monsoon, suggesting that HCHO may not comprehensively represent the shifts in O_3 formation attributed to VOCs. Second, the correlations used in the study are not indicative of causation, but rather reflect the co-variability between O_3 and its precursors, including meteorological factors (Camalier et al., 2007; Porter and Heald, 2019). While these correlations are physically interpretable and well-established in the literature, they do not quantify rates of O_3 production and loss, which are dependent on nonlinear reactions that are not explicitly investigated here. While the utilization of the formaldehyde-to-NOx ratio (FNR) across the study period may provide insight into chemical regimes, this analysis was not performed. Third, some portions of the analysis rely on observations from sites that are not co-located. Each precursor is correlated to O_3 at CP, whereas NO_2 and HCHO are additionally sampled from PGN and TEMPO over CP. This results in

https://doi.org/10.5194/egusphere-2026-3397
Preprint. Discussion started: 29 July 2026

differing spatial footprints and vertical sensitivities which may introduce spatial representativeness biases (Nawaz et al., 2025; Ghahremanloo et al., 2025).

Future studies should incorporate additional VOC measurements, both biogenic and anthropogenic, to better determine diurnal and seasonal variation of O_3-precursor relationships, beyond using HCHO as the sole proxy for VOC chemistry. Direct surface VOC measurements would provide an additional observational context not available in this study and would reduce spatial uncertainty. Moreover, coupling these additional VOC observations with box models, chemical transport modeling and budget calculations of odd-oxygen radicals (HO_x) would help constrain O_3 production and loss rates, and thus offer a more comprehensive analysis of O_3 nonlinear chemistry and its variability across diurnal and seasonal timescales in semi-arid urban environments. By integrating the complementary strengths of both FNR and the glyoxal-to-nitrogen dioxide ratio (GNR), a more robust ozone formation sensitivity (OFS) identification method can be developed (Fan et al., 2025; Tao et al., 2022). These extended analyses could be applied with the recent Ground Level Ozone Research (GLOR) field campaign in Phoenix, Arizona (Fraser et al., 2025). In doing so, these directions would strengthen the chemical regime diagnostics developed here and better constrain O_3 formation in semi-arid urban environments.

Code and data availability

Trace gas measurements and meteorological observations used in this study can be obtained from the U.S. EPA AQS (https://www.epa.gov/aqs) (Last Access: 27 October 2025), Pandonia Global Network (https://downloader.pandonia-global-network.org/#data-availability) (Last Access: 22 October 2025), TEMPO (DOI: 10.5067/IS-40e/TEMPO/NO_2_L3.003 and

https://doi.org/10.5194/egusphere-2026-3397
Preprint. Discussion started: 29 July 2026

10.5067/IS-40e/TEMPO/HCHO_L3.003) (Last Access: 11 December 2025), and Unified Ceilometer Network (https://ucn.cas.hamptonu.edu). (Last Access: 25 December 2025).

Author contributions

MLR, CR, and AFA conceptualized the study and interpreted the data. MLR carried out the analysis and prepared the figures. KP provided the PBLH estimations. MAM provided the land cover class data. All co-authors contributed to reviewing and proofreading of the manuscript.

Competing interests

At least one of the (co-)authors is a member of the editorial board of Atmospheric Chemistry and Physics.

Acknowledgements

This work is supported by NASA grant no. 80NSSC22K1789 and the Arizona Board of Regents (ABOR), Regent's Grant from the Technology and Research Initiative Fund (TRIF).

References

Abad, G. G., Nowlan, C. R., Liu, X., Huiqun Wang, & Chance, K. (2025). *TEMPO Formaldehyde Retrieval Algorithm Theoretical Basis Document*. https://doi.org/10.5067/D0GI6E8K0NO8

Ajayi, T., Amin Mirrezaei, M., F. Arellano, A., S. Robinson, E., & Sorooshian, A. (2025). A long-term (2001–2022) examination of surface ozone concentrations in Tucson, Arizona. *Environmental Science: Atmospheres*, *5*(12), 1326–1340. https://doi.org/10.1039/D5EA00072F

Ajayi, T., Choi, Y., Crosbie, E. C., DiGangi, J. P., Diskin, G. S., Kirschler, S., Moore, R. H., Shook, M. A., Thornhill, K. L., Voigt, C., Winstead, E. L., Ziemba, L. D., & Sorooshian, A. (2025). Can a Weekly Cycle in Pollutants be Observed Offshore the U.S. East Coast with Airborne Measurements? *ACS ES&T Air*, *2*(11), 2704–2717. https://doi.org/10.1021/acsestair.5c00291

Archibald, A. T., Neu, J. L., Elshorbany, Y. F., Cooper, O. R., Young, P. J., Akiyoshi, H., Cox, R. A., Coyle, M., Derwent, R. G., Deushi, M., Finco, A., Frost, G. J., Galbally, I. E., Gerosa, G., Granier, C., Griffiths, P. T., Hossaini, R., Hu, L., Jöckel, P., … Zeng, G. (2020). Tropospheric Ozone Assessment Report. *Elementa: Science of the Anthropocene*, *8*(1), 034. https://doi.org/10.1525/elementa.2020.034

Ayazpour, Z., Tao, S., Li, D., Scarino, A. J., Kuehn, R. E., and Sun, K. (2023). Estimates of the spatially complete, observational-data-driven planetary boundary layer height over the contiguous United States, Atmos. Meas. Tech., 16, 563–580, https://doi.org/10.5194/amt-16-563-2023.

Betito, G., Arellano, A., & Sorooshian, A. (2024). Influence of Transboundary Pollution on the Variability of Surface Ozone Concentrations in the Desert Southwest of the U.S.: Case Study for Arizona. *Atmosphere*, *15*(4), 401. https://doi.org/10.3390/atmos15040401

Borbon, A., Gilman, J. B., Kuster, W. C., Grand, N., Chevaillier, S., Colomb, A., Dolgorouky, C., Gros, V., Lopez, M., Sarda-Esteve, R., Holloway, J., Stutz, J., Petetin, H., McKeen, S., Beekmann, M., Warneke, C., Parrish, D. D., & De Gouw, J. A. (2013). Emission ratios of anthropogenic volatile organic compounds in northern mid-latitude megacities:

https://doi.org/10.5194/egusphere-2026-3397
Preprint. Discussion started: 29 July 2026

Observations versus emission inventories in Los Angeles and Paris. *Journal of Geophysical Research: Atmospheres*, *118*(4), 2041–2057. https://doi.org/10.1002/jgrd.50059

Caicedo, V., Rappenglück, B., Lefer, B., Morris, G., Toledo, D., & Delgado, R. (2017). Comparison of aerosol lidar retrieval methods for boundary layer height detection using ceilometer aerosol backscatter data. *Atmospheric Measurement Techniques*, *10*(4), 1609–1622. https://doi.org/10.5194/amt-10-1609-2017

Camalier, L., Cox, W., & Dolwick, P. (2007). The effects of meteorology on ozone in urban areas and their use in assessing ozone trends. *Atmospheric Environment*, *41*(33), 7127–7137. https://doi.org/10.1016/j.atmosenv.2007.04.061

Caputi, D. J., Faloona, I., Trousdell, J., Smoot, J., Falk, N., and Conley, S. (2019). Residual layer ozone, mixing, and the nocturnal jet in California's San Joaquin Valley, Atmos. Chem. Phys., 19, 4721–4740, https://doi.org/10.5194/acp-19-4721-2019.

Caputi, D.J., Trousdell, J., Mehrotra, S. *et al.* (2023). Entrainment Rates and Their Synoptic Dependence on Wind Speed Aloft in California's Central Valley. *Boundary-Layer Meteorol* 186, 505–532, https://doi.org/10.1007/s10546-022-00770-1.

Cede, A., Tiefengraber, M., Gebetsberger, M., & Lind, E. (2025, January 20). *Pandonia Global Network Data Products Readme Document*. Pandonia Global Network. Retrieved from https://www.pandonia-global-network.org.

Chatfield, R. B., Ren, X., Brune, W., & Schwab, J. (2010). Controls on urban ozone production rate as indicated by formaldehyde oxidation rate and nitric oxide. *Atmospheric Environment, Atmospheric Chemical Mechanisms: Selected Papers from the 2008 Conference*, *44*(40), 5395–5406. https://doi.org/10.1016/j.atmosenv.2010.08.056

Cui, K., Liu, D., Chen, Y., Wang, H., Zu, F., Wang, Z., & Shen, L. (2026). The planetary boundary layer top as a valve: Unraveling bidirectional aerosol transport. *Environmental Research*, *296*, 123986. https://doi.org/10.1016/j.envres.2026.123986

De Smedt, I., Stavrakou, T., Hendrick, F., Danckaert, T., Vlemmix, T., Pinardi, G., Theys, N., Lerot, C., Gielen, C., Vigouroux, C., Hermans, C., Fayt, C., Veefkind, P., Müller, J.-F., and Van Roozendael, M. (2015). Diurnal, seasonal and long-term variations of global formaldehyde columns inferred from combined OMI and GOME-2 observations. Atmospheric Chemistry and Physics, 15(22), 12519–12545. https://doi.org/10.5194/acp-15-12519-2015

Di, Q., Wang, Y., Zanobetti, A., Wang, Y., Koutrakis, P., Choirat, C., Dominici, F., & Schwartz, J. D. (2017). Air Pollution and Mortality in the Medicare Population. *New England Journal of Medicine*, *376*(26), 2513–2522. https://doi.org/10.1056/NEJMoa1702747

Du, Q., Zhao, C., Zhang, M., Dong, X., Chen, Y., Liu, Z., Hu, Z., Zhang, Q., Li, Y., Yuan, R., and Miao, S. (2020). Modeling diurnal variation of surface $PM_{2.5}$ concentrations over East China with WRF-Chem: impacts from boundary-layer mixing and anthropogenic emission, Atmos. Chem. Phys., 20, 2839–2863, https://doi.org/10.5194/acp-20-2839-2020.

Fan, J., Yu, C., Li, Y., Zhang, Y., Fan, M., Tao, J., & Chen, L. (2025). Comparison of FNR and GNR Based on TROPOMI Satellite Data for Ozone Sensitivity Analysis in Chinese Urban Agglomerations. *Remote Sensing*, *17*(19), 3321. https://doi.org/10.3390/rs17193321

Finlayson-Pitts, B. J., & Pitts, J. N. (1993). Atmospheric Chemistry of Tropospheric Ozone Formation: Scientific and Regulatory Implications. *Air & Waste*, *43*(8), 1091–1100. https://doi.org/10.1080/1073161X.1993.10467187

Fiore, A. M., Naik, V., and Leibensperger, E. M. (2015). Air quality and climate connections. Journal of the Air & Waste Management Association, 65(6), 645–685. https://doi.org/10.1080/10962247.2015.1040526

Fiore, A. M., Naik, V., Spracklen, D. V., Steiner, A., Unger, N., Prather, M., Bergmann, D., Cameron-Smith, P. J., Cionni, I., Collins, W. J., Dalsøren, S., Eyring, V., Folberth, G. A., Ginoux, P., Horowitz, L. W., Josse, B., Lamarque, J.-F., MacKenzie, I. A., Nagashima, T., O'Connor, F. M., Righi, M., Rumbold, S. T., Shindell, D. T., Skeie, R. B., Sudo, K., Szopa, S., Takemura, T., and Zeng, G. (2012). Global air quality and climate. Chemical Society Reviews, 41(19), 6663–6683. https://doi.org/10.1039/c2cs35095e

Fishman, J., Bowman, K. W., Burrows, J. P., Richter, A., Chance, K. V., Edwards, D. P., Martin, R. V., Morris, G. A., Pierce, R. B., Ziemke, J. R., Al-Saadi, J. A., Creilson, J. K., Schaack, T. K., and Thompson, A. M. (2008). Remote sensing of tropospheric pollution from space. Bulletin of the American Meteorological Society, 89(6), 805–821. https://doi.org/10.1175/2008BAMS2526.1

Foskinis, R., Gini, M. I., Kokkalis, P., Diapouli, E., Vratolis, S., Granakis, K., Zografou, O., Komppula, M., Vakkari, V., Nenes, A., Papayannis, A., & Eleftheriadis, K. (2024). On the relation between the planetary boundary layer height

https://doi.org/10.5194/egusphere-2026-3397
Preprint. Discussion started: 29 July 2026

and in situ surface observations of atmospheric aerosol pollutants during spring in an urban area. *Atmospheric Research*, *308*, 107543. https://doi.org/10.1016/j.atmosres.2024.107543

Fraser, M.P., Arellano, A.F., Herckes, P., Robinson, E., Sorooshian, A., 2025. Feeling the heat: Ground Level Ozone Research (GLOR) ramps up in Maricopa County. EM Mag. Air Waste Manag. Assoc. 21–25.

Fu, T.-M., & Tian, H. (2019). Climate Change Penalty to Ozone Air Quality: Review of Current Understandings and Knowledge Gaps. *Current Pollution Reports*, *5*(3), 159–171. https://doi.org/10.1007/s40726-019-00115-6

Ghahremanloo, M., Nowlan, C., González Abad, G., Garraffo, C., Liu, X., Wang, H., Henderson, B., Baumann, E., Valin, L., Geddes, J. A., & Zhao, X. (2025). Comprehensive Analysis of Bias in TEMPO NO_2 Column Densities Through Pandora Observations. *Journal of Geophysical Research: Atmospheres*, *130*(15), e2025JD044150. https://doi.org/10.1029/2025JD044150

Greenslade, M., Guo, Y., Betito, G., Mirrezaei, M. A., Roychoudhury, C., Arellano, A. F., & Sorooshian, A. (2024). On ozone's weekly cycle for different seasons in Arizona. *Atmospheric Environment*, *334*, 120703. https://doi.org/10.1016/j.atmosenv.2024.120703

Guo, Y., Mirrezaei, M. A., Sorooshian, A., & Arellano, A. F. (2025). Source contribution to ozone pollution during June 2021 fire events in Arizona: Insights from WRF-Chem-tagged O_3 and CO. *Atmospheric Chemistry and Physics*, *25*(11), 5591–5616. https://doi.org/10.5194/acp-25-5591-2025

Harkey, M., and Holloway, T. (2024). Simulated surface-column NO_2 connections for satellite applications. Journal of Geophysical Research: Atmospheres, 129, e2024JD041912. https://doi.org/10.1029/2024JD041912

Hearn, A. G. (1961). The absorption of ozone in the ultra-violet and visible regions of the spectrum. Proceedings of the Physical Society, 78(5), 932–940. https://doi.org/10.1088/0370-1328/78/5/340

Herman, J., Cede, A., Spinei, E., Mount, G., Tzortziou, M., & Abuhassan, N. (2009). NO_2 column amounts from ground-based Pandora and MFDOAS spectrometers using the direct-sun DOAS technique: Intercomparisons and application to OMI validation. *Journal of Geophysical Research: Atmospheres*, *114*(D13), 2009JD011848. https://doi.org/10.1029/2009JD011848

Homer, C., Dewitz, J., Jin, S., Xian, G., Costello, C., Danielson, P., Gass, L., Funk, M., Wickham, J., Stehman, S., Auch, R., and Riitters, K. (2020). Conterminous United States land cover change patterns 2001–2016 from the 2016 National Land Cover Database. ISPRS Journal of Photogrammetry and Remote Sensing, 162, 184–199. https://doi.org/10.1016/j.isprsjprs.2020.02.019

Jardine, K., Harley, P., Karl, T., Guenther, A., Lerdau, M., and Mak, J. E. (2010). Volatile organic compound emissions from Larrea tridentata (creosotebush). Atmospheric Chemistry and Physics, 10(24), 12191–12206. https://doi.org/10.5194/acp-10-12191-2010

Jin, X., Fiore, A., Boersma, K. F., Smedt, I. D., & Valin, L. (2020). Inferring Changes in Summertime Surface Ozone–NO_x–VOC Chemistry over U.S. Urban Areas from Two Decades of Satellite and Ground-Based Observations. *Environmental Science & Technology*, *54*(11), 6518–6529. https://doi.org/10.1021/acs.est.9b07785

Jin, X., Cai, X., Yu, M., Song, Y., Wang, X., Zhang, H., and Zhu, T. (2022). Regional $PM_{2.5}$ pollution confined by atmospheric internal boundaries in the North China Plain: boundary layer structures and numerical simulation, Atmos. Chem. Phys., 22, 11409–11427, https://doi.org/10.5194/acp-22-11409-2022.

Jin, X., Yang, Y., Gonzalez Abad, G., Nowlan, C., & Liu, X. (2025). Observing the Diurnal Variations of Ozone-NO_x -VOC Chemistry Over the U.S. From the Geostationary TEMPO Instrument. *Geophysical Research Letters*, *52*(14), e2025GL116394. https://doi.org/10.1029/2025GL116394

Kaser, L., Patton, E. G., Pfister, G. G., Weinheimer, A. J., Montzka, D. D., Flocke, F., Thompson, A. M., Stauffer, R. M., & Halliday, H. S. (2017). The effect of entrainment through atmospheric boundary layer growth on observed and modeled surface ozone in the Colorado Front Range. *Journal of Geophysical Research: Atmospheres*, *122*(11), 6075–6093. https://doi.org/10.1002/2016JD026245

Kleinman, L. I., Daum, P. H., Lee, Y. -N., Nunnermacker, L. J., Springston, S. R., Weinstein-Lloyd, J., & Rudolph, J. (2005). A comparative study of ozone production in five U.S. metropolitan areas. *Journal of Geophysical Research: Atmospheres*, *110*(D2), 2004JD005096. https://doi.org/10.1029/2004JD005096

Knepp, T. N., Szykman, J. J., Long, R., Duvall, R. M., Krug, J., Beaver, M., Cavender, K., Kronmiller, K., Wheeler, M., Delgado, R., Hoff, R., Berkoff, T., Olson, E., Clark, R., Wolfe, D., Van Gilst, D., and Neil, D. (2015). Estimating surface NO_2 and SO2 mixing ratios from fast-response total column observations and potential application to

https://doi.org/10.5194/egusphere-2026-3397
Preprint. Discussion started: 29 July 2026

geostationary missions. Journal of Atmospheric Chemistry, 72(3), 261–286. https://doi.org/10.1007/s10874-013-9257-6

Lamsal, L. N., Martin, R. V., Van Donkelaar, A., Steinbacher, M., Celarier, E. A., Bucsela, E., Dunlea, E. J., & Pinto, J. P. (2008). Ground-level nitrogen dioxide concentrations inferred from the satellite-borne Ozone Monitoring Instrument. *Journal of Geophysical Research: Atmospheres*, *113*(D16), 2007JD009235. https://doi.org/10.1029/2007JD009235

Leys, C., Ley, C., Klein, O., Bernard, P., & Licata, L. (2013). Detecting outliers: Do not use standard deviation around the mean, use absolute deviation around the median. *Journal of Experimental Social Psychology*, *49*(4), 764–766. https://doi.org/10.1016/j.jesp.2013.03.013

Lorente, A., Folkert Boersma, K., Yu, H., Dörner, S., Hilboll, A., Richter, A., Liu, M., Lamsal, L. N., Barkley, M., De Smedt, I., Van Roozendael, M., Wang, Y., Wagner, T., Beirle, S., Lin, J.-T., Krotkov, N., Stammes, P., Wang, P., Eskes, H. J., and Krol, M. (2017). Structural uncertainty in air mass factor calculation for NO_2 and HCHO satellite retrievals. Atmospheric Measurement Techniques, 10, 759–782. https://doi.org/10.5194/amt-10-759-2017

Malloy, J.W. (2018). Atmospheric patterns in relationship with observed ozone concentrations in the Phoenix, Arizona, metropolitan area during the North American Monsoon. *Atmospheric Environment*, *191*, 64–69. https://doi.org/10.1016/j.atmosenv.2018.08.001

Malloy, J.W. and Cerveny, R.S. (2019). Atmospheric Composite Sounding Analysis as a Forecasting Tool for Ozone Accumulation in a Semiarid Metropolitan Area during the North American Monsoon: Phoenix, Arizona. *Weather and Forecasting*, 34(4), 887–904. https://doi.org/10.1175/WAF-D-18-0204.1.

Monks, P. S., Archibald, A. T., Colette, A., Cooper, O., Coyle, M., Derwent, R., Fowler, D., Granier, C., Law, K. S., Mills, G. E., Stevenson, D. S., Tarasova, O., Thouret, V., Von Schneidemesser, E., Sommariva, R., Wild, O., & Williams, M. L. (2015). Tropospheric ozone and its precursors from the urban to the global scale from air quality to short-lived climate forcer. *Atmospheric Chemistry and Physics*, *15*(15), 8889–8973. https://doi.org/10.5194/acp-15-8889-2015

Nawaz, M. O., Huber, D. E., Kerr, G. H., Judd, L. M., Acker, S. J., & Goldberg, D. L. (2025). A Comparative Analysis of TEMPO NO_2 Remote Sensing With Surface-Level Monitoring Through Diurnal and Seasonal Trends, Meteorology, and Monitor Characteristics. *Journal of Geophysical Research: Atmospheres*, *130*(20), e2025JD043923. https://doi.org/10.1029/2025JD043923

Nowlan, C. R., Abad, G. G., Liu, X., Huiqun Wang, & Chance, K. (2025). *TEMPO Nitrogen Dioxide Retrieval Algorithm Theoretical Basis Document*. https://doi.org/10.5067/WX026254FI2U

Nussbaumer, C. M., & Cohen, R. C. (2020). The Role of Temperature and NO_x in O_3 Trends in the Los Angeles Basin. *Environmental Science & Technology*, *54*(24), 15652–15659. https://doi.org/10.1021/acs.est.0c04910

Parakkat, L., Hilario, M. R. A., Mirrezaei, M. A., Robinson, E. S., Arellano, A., & Sorooshian, A. (2025). Ozone concentrations and influential variables during heat waves over two desert cities in the Southwest U.S. *Environmental Research Communications*, *7*(12), 125008. https://doi.org/10.1088/2515-7620/ae238d

Porter, W. C., and Heald, C. L. (2019). The mechanisms and meteorological drivers of the summertime ozone–temperature relationship. Atmospheric Chemistry and Physics, 19, 13367–13381. https://doi.org/10.5194/acp-19-13367-2019

Pusede, S. E., & Cohen, R. C. (2012). On the observed response of ozone to NO_x and VOC reactivity reductions in San Joaquin Valley California 1995–present. *Atmospheric Chemistry and Physics*, *12*(18), 8323–8339. https://doi.org/10.5194/acp-12-8323-2012

Pusede, S. E., Steiner, A. L., & Cohen, R. C. (2015). Temperature and Recent Trends in the Chemistry of Continental Surface Ozone. *Chemical Reviews*, *115*(10), 3898–3918. https://doi.org/10.1021/cr5006815

Qu, H., Wang, Y., Zhang, R., Liu, X., Huey, L. G., Sjostedt, S., Zeng, L., Lu, K., Wu, Y., Shao, M., Hu, M., Tan, Z., Fuchs, H., Broch, S., Wahner, A., Zhu, T., & Zhang, Y. (2021). Chemical Production of Oxygenated Volatile Organic Compounds Strongly Enhances Boundary-Layer Oxidation Chemistry and Ozone Production. *Environmental Science & Technology*, *55*(20), 13718–13727. https://doi.org/10.1021/acs.est.1c04489

Ramya, A., Dhevagi, P., Poornima, R., Avudainayagam, S., Watanabe, M., & Agathokleous, E. (2023). Effect of ozone stress on crop productivity: A threat to food security. *Environmental Research*, *236*, 116816. https://doi.org/10.1016/j.envres.2023.116816

Rawat, P., Crawford, J. H., Travis, K. R., Judd, L. M., Demetillo, M. A. G., Valin, L. C., Szykman, J. J., Whitehill, A., Baumann, E., & Hanisco, T. F. (2025). Maximizing the scientific application of Pandora column observations of

https://doi.org/10.5194/egusphere-2026-3397
Preprint. Discussion started: 29 July 2026

HCHO and NO_2. *Atmospheric Measurement Techniques*, *18*(13), 2899–2917. https://doi.org/10.5194/amt-18-2899-2025

Rawat, P., Travis, K. R., Henderson, B., Crawford, J. H., Judd, L. M., Demetillo, M. A. G., Lee, T. C., Flittner, D. E., Szykman, J. J., Valin, L. C., Whitehill, A., Baumann, E., Hanisco, T. F., Pandey, A., Abad, G. G., Nowlan, C. R., Liu, X., & Chance, K. (2026). Spatiotemporal Assessment of the TEMPO Formaldehyde Column Retrieval Using the Pandonia Global Network. *Journal of Geophysical Research: Atmospheres*, *131*(2), e2025JD044788. https://doi.org/10.1029/2025JD044788

Sebol, A., Wolfe, G., Canty, T., St. Clair, J., Delaria, E., Kaiser, J., Desai, N., Rollins, A., Waxman, E., Zuraski, K., Place, B., Pandey, A., Singh, A., Ring, A., Gatebe, C., & Dean-Day, J. (2025). *Evaluation of Pandora HCHO and* NO_2 *with Airborne In Situ Observations*. Gases/Remote Sensing/Validation and Intercomparisons. https://doi.org/10.5194/egusphere-2025-5261

Seibert, P. (2000). Review and intercomparison of operational methods for the determination of the mixing height. *Atmospheric Environment*, *34*(7), 1001–1027. https://doi.org/10.1016/S1352-2310(99)00349-0

Sillman, S. (2002). Chapter 12 The relation between ozone, NO_x and hydrocarbons in urban and polluted rural environments. In *Developments in Environmental Science* (Vol. 1, pp. 339–385). Elsevier. https://doi.org/10.1016/S1474-8177(02)80015-8

Snyder, K. A., & Tartowski, S. L. (2006). Multi-scale temporal variation in water availability: Implications for vegetation dynamics in arid and semi-arid ecosystems. *Journal of Arid Environments*, *65*(2), 219–234. https://doi.org/10.1016/j.jaridenv.2005.06.023

Sorooshian, A., Arellano, A. F., Fraser, M. P., Herckes, P., Betito, G., Betterton, E. A., Braun, R. A., Guo, Y., Mirrezaei, M. A., & Roychoudhury, C. (2024). Ozone in the Desert Southwest of the United States: A Synthesis of Past Work and Steps Ahead. *ACS ES&T Air*, *1*(2), 62–79. https://doi.org/10.1021/acsestair.3c00033

Souri, A. H., Johnson, M. S., Wolfe, G. M., Crawford, J. H., Fried, A., Wisthaler, A., Brune, W. H., Blake, D. R., Weinheimer, A. J., Verhoelst, T., Compernolle, S., Pinardi, G., Vigouroux, C., Langerock, B., Choi, S., Lamsal, L., Zhu, L., Sun, S., Cohen, R. C., Min, K.-E., Cho, C., Philip, S., Liu, X., and Chance, K. (2023). Characterization of errors in satellite-based $HCHO/NO_2$ tropospheric column ratios with respect to chemistry, column-to-PBL translation, spatial representation, and retrieval uncertainties, Atmos. Chem. Phys., 23, 1963–1986, https://doi.org/10.5194/acp-23-1963-2023.

Stathopoulou, E., Mihalakakou, G., Santamouris, M., & Bagiorgas, H. S. (2008). On the impact of temperature on tropospheric ozone concentration levels in urban environments. *Journal of Earth System Science*, *117*(3), 227–236. https://doi.org/10.1007/s12040-008-0027-9

Stavrakou, T., Müller, J.-F., Bauwens, M., De Smedt, I., Van Roozendael, M., De Mazière, M., Vigouroux, C., Hendrick, F., George, M., Clerbaux, C., Coheur, P.-F., & Guenther, A. (2015). How consistent are top-down hydrocarbon emissions based on formaldehyde observations from GOME-2 and OMI? *Atmospheric Chemistry and Physics*, *15*(20), 11861–11884. https://doi.org/10.5194/acp-15-11861-2015

Stull, R. B. (2012). *An introduction to boundary layer meteorology*. Springer Science & Business Media.

Su, T., Li, Z., and Kahn, R. (2018). Relationships between the planetary boundary layer height and surface pollutants derived from lidar observations over China: regional pattern and influencing factors, Atmos. Chem. Phys., 18, 15921–15935, https://doi.org/10.5194/acp-18-15921-2018.

Sullivan, J. T., Berkoff, T., Gronoff, G., Knepp, T., Pippin, M., Allen, D., Twigg, L., Swap, R., Tzortziou, M., Thompson, A. M., Stauffer, R. M., Wolfe, G. M., Flynn, J., Pusede, S. E., Judd, L. M., Moore, W., Baker, B. D., Al-Saadi, J., and McGee, T. J. (2019). The Ozone Water-Land Environmental Transition Study (OWLETS): An innovative strategy for understanding Chesapeake Bay pollution events. Bulletin of the American Meteorological Society, 100(2), 291–306. https://doi.org/10.1175/BAMS-D-18-0025.1

Tao, M., Fiore, A. M., Jin, X., Schiferl, L. D., Commane, R., Judd, L. M., Janz, S., Sullivan, J. T., Miller, P. J., Karambelas, A., Davis, S., Tzortziou, M., Valin, L., Whitehill, A., Civerolo, K., and Tian, Y. (2022). Investigating changes in ozone formation chemistry during summertime pollution events over the Northeastern United States. Environmental Science & Technology, 56(22), 15312–15327. https://doi.org/10.1021/acs.est.2c02972

Tao, M., Fiore, A. M., Jin, X., Schiferl, L. D., Commane, R., Judd, L. M., Janz, S., Sullivan, J. T., Miller, P. J., Karambelas, A., Davis, S., Tzortziou, M., Valin, L., Whitehill, A., Civerolo, K., and Tian, Y. (2025). Insights into summertime

https://doi.org/10.5194/egusphere-2026-3397
Preprint. Discussion started: 29 July 2026

surface ozone formation from diurnal variations in formaldehyde and nitrogen dioxide along a transect through New York City. Journal of Geophysical Research: Atmospheres, 130, e2024JD040922. https://doi.org/10.1029/2024JD040922

Valin, L. C., Russell, A. R., Hudman, R. C., & Cohen, R. C. (2011). Effects of model resolution on the interpretation of satellite NO_2 observations. *Atmospheric Chemistry and Physics*, *11*(22), 11647–11655. https://doi.org/10.5194/acp-11-11647-2011

Valin, L. C., Fiore, A. M., Chance, K., & González Abad, G. (2016). The role of OH production in interpreting the variability of CH_2O columns in the southeast U.S. *Journal of Geophysical Research: Atmospheres*, *121*(1), 478–493. https://doi.org/10.1002/2015JD024012

Vaisala Oyj: BL-Matlab User's Guide v0.98, Vaisala Oyj, Helsinki, Finland, 2011. (2011). Vaisala Oyj.

Veefkind, J. P., Aben, I., McMullan, K., Förster, H., De Vries, J., Otter, G., Claas, J., Eskes, H. J., De Haan, J. F., Kleipool, Q., Van Weele, M., Hasekamp, O., Hoogeveen, R., Landgraf, J., Snel, R., Tol, P., Ingmann, P., Voors, R., Kruizinga, B., … Levelt, P. F. (2012). TROPOMI on the ESA Sentinel-5 Precursor: A GMES mission for global observations of the atmospheric composition for climate, air quality and ozone layer applications. *Remote Sensing of Environment*, *120*, 70–83. https://doi.org/10.1016/j.rse.2011.09.027

Verhoelst, T., Compernolle, S., Pinardi, G., Lambert, J.-C., Eskes, H. J., Eichmann, K.-U., Fjæraa, A. M., Granville, J., Niemeijer, S., Cede, A., Tiefengraber, M., Hendrick, F., Pazmiño, A., Bais, A., Bazureau, A., Boersma, K. F., Bognar, K., Dehn, A., Donner, S., ... Zehner, C. (2021). Ground-based validation of the Copernicus Sentinel-5P TROPOMI NO_2 measurements with the NDACC ZSL-DOAS, MAX-DOAS and Pandonia global networks. Atmospheric Measurement Techniques, 14(1), 481–510. https://doi.org/10.5194/amt-14-481-2021

Volkamer, R., Molina, L. T., Molina, M. J., Shirley, T., & Brune, W. H. (2005). DOAS measurement of glyoxal as an indicator for fast VOC chemistry in urban air. *Geophysical Research Letters*, *32*(8), 2005GL022616. https://doi.org/10.1029/2005GL022616

von Schneidemesser, E., Monks, P. S., Allan, J. D., Bruhwiler, L., Forster, P., Fowler, D., Lauer, A., Morgan, W. T., Paasonen, P., Righi, M., Sindelarova, K., and Sutton, M. A. (2015). Chemistry and the linkages between air quality and climate change. Chemical Reviews, 115(10), 3856–3897. https://doi.org/10.1021/acs.chemrev.5b00089

Wang, P., Holloway, T., Bindl, M., Harkey, M., & De Smedt, I. (2022). Ambient Formaldehyde over the United States from Ground-Based (AQS) and Satellite (OMI) Observations. *Remote Sensing*, *14*(9), Article 9. https://doi.org/10.3390/rs14092191

Wiegner, M. and Geiß, A. (2012). Aerosol profiling with the Jenoptik ceilometer CHM15kx, *Atmos. Meas. Tech.*, *5*, 1953–1964, https://doi.org/10.5194/amt-5-1953-2012.

Wilcox, R. R. (2016). Comparing dependent robust correlations. *British Journal of Mathematical and Statistical Psychology*, *69*(3), 215–224. https://doi.org/10.1111/bmsp.12069

Wolfe, G. M., Kaiser, J., Hanisco, T. F., Keutsch, F. N., De Gouw, J. A., Gilman, J. B., Graus, M., Hatch, C. D., Holloway, J., Horowitz, L. W., Lee, B. H., Lerner, B. M., Lopez-Hilifiker, F., Mao, J., Marvin, M. R., Peischl, J., Pollack, I. B., Roberts, J. M., Ryerson, T. B., … Warneke, C. (2016). Formaldehyde production from isoprene oxidation across NO_x regimes. *Atmospheric Chemistry and Physics*, *16*(4), 2597–2610. https://doi.org/10.5194/acp-16-2597-2016

Youn, J., Wang, Z., Wonaschütz, A., Arellano, A., Betterton, E. A., & Sorooshian, A. (2013). Evidence of aqueous secondary organic aerosol formation from biogenic emissions in the North American Sonoran Desert. *Geophysical Research Letters*, *40*(13), 3468–3472. https://doi.org/10.1002/grl.50644

Zhu, L., Jacob, D. J., Keutsch, F. N., Mickley, L. J., Scheffe, R., Strum, M., González Abad, G., Chance, K., Yang, K., Rappenglück, B., Millet, D. B., Baasandorj, M., Jaeglé, L., and Shah, V. (2017). Formaldehyde (HCHO) as a hazardous air pollutant: Mapping surface air concentrations from satellite and inferring cancer risks in the United States. Environmental Science & Technology, 51(10), 5650–5658. https://doi.org/10.1021/acs.est.7b01356

Zoogman, P., Liu, X., Suleiman, R. M., Pennington, W. F., Flittner, D. E., Al-Saadi, J. A., Hilton, B. B., Nicks, D. K., Newchurch, M. J., Carr, J. L., Janz, S. J., Andraschko, M. R., Arola, A., Baker, B. D., Canova, B. P., Chan Miller, C., Cohen, R. C., Davis, J. E., Dussault, M. E., … Chance, K. (2017). Tropospheric emissions: Monitoring of pollution (TEMPO). *Journal of Quantitative Spectroscopy and Radiative Transfer*, *186*, 17–39. https://doi.org/10.1016/j.jqsrt.2016.05.008